Coordinated cerebellar climbing fiber activity signals learned sensorimotor predictions

William Heffley II[1], Eun Young Song[1], Ziye Xu[1], Benjamin Taylor[1], Mary Anne Hughes[1], Andrew McKinney[1,2,3], Mati Joshua[1,4] and Court Hull[1]

[1]Department of Neurobiology, Duke University Medical School, Durham, United States
[2]Neuroscience Department, Baylor College of Medicine, Houston, United States
[3]Duncan Neurological Research Institute at Texas Children's Hospital, Houston, United States
[4]Department of Medical Neurobiology, The Hebrew University, Hadassah Medical School, Jerusalem, Israel

Correspondence:

Dr. Court Hull
Duke University Medical School
Dept. of Neurobiology
311 Research Drive
Durham, NC 27710

Email: Hull@neuro.duke.edu
Phone: 919-613-0927

Acknowledgements:
This work was supported by grants from the NIH NINDS (5R01NS096289-02), the Sloan Foundation, and the Whitehall Foundation. We thank Dr. Lindsey Glickfeld for helpful discussions and input on calcium imaging approaches and analyses, Drs. Stephen Lisberger, Greg Field, Kevin Franks and Fan Wang for feedback on early versions of this manuscript, and members of the Hull and Glickfeld labs for input and technical assistance throughout the project.

Abstract

The prevailing model of cerebellar learning states that climbing fibers (CFs) are both driven by, and serve to correct, erroneous motor output. However, this model is grounded largely in studies of behaviors that utilize hardwired neural pathways to link sensory input to motor output. To test whether this model applies to more flexible learning regimes that require arbitrary sensorimotor associations, we have developed a cerebellar-dependent motor learning paradigm compatible with both mesoscale and single dendrite resolution calcium imaging in mice. Here, we find that CFs are preferentially driven by and more time-locked to correctly executed movements and other task parameters that predict reward outcome, exhibiting widespread correlated activity within parasagittal processing zones that is governed by these predictions. Together, such CF activity patterns are well-suited to drive learning by providing predictive instructional input that is consistent with an unsigned reinforcement learning signal but does not rely exclusively on motor errors.

Introduction

A key role of the cerebellum is to form predictive associations between sensory inputs and motor outputs. These sensorimotor predictions are critical for generating well-timed and accurate movements, and in the absence of cerebellar function, the lack of such predictive motor output severely impairs our ability to generate coordinated responses to stimuli in the external world.

Classic models posit that the cerebellum generates sensorimotor predictions according to a supervised learning rule[1-3]. According to such models, projections from the inferior olive called climbing fibers are thought to signal motor errors, thus providing information to Purkinje cells about discrepancies between the expected consequences of a motor command and subsequent sensory feedback. To correct erroneous motor output, the climbing fibers instruct heterosynaptic long-term depression[4-6] by producing powerful regenerative calcium transients[7-9] in Purkinje cell dendrites called complex spikes[10, 11]. In so doing, climbing fibers are thought to appropriately update the cerebellar forward internal model with revised sensorimotor predictions.

This supervised error-signaling framework provides a compelling explanation for climbing fiber activity in a variety of simple behaviors, such as classical conditioning (e.g. eyeblink conditioning) and adaptation (e.g. vestibulo-ocular reflex gain changes)[12-14] paradigms. Such behaviors typically rely on a yoked relationship between unconditioned sensory input and motor output, allowing the cerebellum to utilize signals from hardwired pathways to drive learning. Hence, the climbing fibers can instruct learning by responding to an unconditioned stimulus (e.g. periocular eye puff or retinal slip) that produces the same movement requiring modification (e.g. eyelid closure or eye movement).

However, many forms of motor learning do not involve modifications to motor programs linked directly to an unconditioned stimulus and response. Instead, the correct association between sensory input and motor output must be learned through experience, and the sensory information necessary for learning may have no direct relationship to the movement that requires modification. Such abstract associations necessitate that learning cannot be achieved by input from hardwired sensorimotor pathways alone. Under such conditions, where an unconditioned stimulus and response alone does not contain sufficient information to guide learning, it is unclear how a supervised error signal could be generated, or whether such a learning rule could account for either climbing fiber activity or the cerebellar contribution to learning.

To test how the climbing fiber system is engaged under conditions where the sensory and motor signals necessary to drive learning are not innate, we have established a cerebellar-dependent behavioral paradigm compatible with population level *in vivo* calcium imaging, optogenetic and electrophysiological approaches. Using this paradigm, we reveal two key features of cerebellar climbing fiber (CF) driven complex spiking. First, we find that complex spiking cannot be accounted for by a simple error-based supervised learning model. Instead, complex spiking can signal learned, task specific predictions about the likely outcome of movement in a manner that is consistent with a reinforcement learning signal. Second, population level recordings reveal that while complex spiking is correlated within and across parasagittal zones, these correlations also depend on behavioral context. While previous measurements have shown increased correlations in complex spiking in response to sensory input or motor output[15-18], and have suggested an important role for synchrony in downstream processing and motor learning[19], our results reveal that such modulation can vary for identical movements depending on behavioral relevance. Hence, these data reveal key features of cerebellar CF activity that differ significantly from classically studied cerebellar behaviors, and suggest an extension to current models of cerebellar learning in order to account for the role of complex spiking in tasks that require abstract sensorimotor associations.

Results:

To determine the conditions under which climbing fiber driven complex spiking occurs during a motor learning regime that requires an arbitrary sensorimotor association, we first designed an appropriate task. An important feature of the task design is to specifically engage neurons near the dorsal surface of the cerebellum, thereby allowing for visualization of complex spikes at the population level via calcium imaging. Hence, we used optogenetics to functionally map the midlateral dorsal surface of the mouse cerebellum according to the motor output produced by spatially defined populations of Purkinje cells (PCs). To do so, we expressed Archaerhodopsin (Arch) using a transgenic approach (methods) in cerebellar PCs (Fig. 1A), and

109 used an external fiber coupled laser to transiently suppress PCs near the dorsal surface of the
110 cerebellum (Fig. 1B). Consistent with previous work[20], we identified a population of superficial
111 PCs in lobule simplex capable of driving ipsilateral forelimb movements either during optogenetic
112 silencing with Arch or following a brief train of electrical simulation (Fig. 1, Supp. Fig. 1, Supp.
113 Movie 1). *In vivo* single unit recordings confirmed that our optogenetic stimulation was effective
114 in silencing superficial PCs at the threshold for driving forelimb movement (~20 mW) up to a depth
115 of 500 μm (Fig. 1B).
116
117 **A cerebellar dependent sensorimotor association learning task**
118 Based on these results, we designed a sensorimotor association task involving forelimb
119 movement, with the rationale that the cerebellar contribution to learning in such a task should
120 necessarily involve the PCs capable of driving such movements. This task contains two discrete
121 conditions; one where motor output is reactive ('cue reaction'), and another where motor output
122 becomes predictive with learning ('cue prediction'). In both task variations, head restrained, water
123 deprived mice are trained to self-initiate trials by depressing a lever, and to release the lever in
124 response to a visual cue (Fig. 1C,D).
125 In the cue reaction condition, trial-to-trial variability in the timing of the visual cue (Fig.
126 1E,G- "random cue delay") is imposed to necessitate that mice employ reactive forelimb
127 responses. In this regime, lever release reaction times are reflective of the latency for sensory
128 integration[21] and remain constant throughout each session (ΔRT = 1.1 $\pm$ 9.3 ms, n=26 sessions,
129 7 mice, Supp. Movie 2).
130 In the cue prediction condition, by presenting the visual cue with a constant delay on every
131 trial, mice learn to predict the timing of the cue and adjust their motor responses to more closely
132 approximate the time of cue (Fig. 1F,G, ΔRT 500ms cue delay = 154.5 $\pm$ 13.6 ms, n=44 sessions,
133 10 mice). Moreover, learning occurs within a single training session (90 min., 309-700 trials), is
134 retained across days (Supp. Fig. 2A), and can be extinguished by returning mice to the cue
135 reaction paradigm (Supp. Fig. 2C,D). In addition, we find that learning depends on the duration
136 of the cue delay: maximal learning occurs at short cue delays (e.g. 500 ms) and little or no learning
137 occurs for cue delays greater than 1.5 seconds (Fig. 1H; one-way ANOVA, main effect of cue
138 delay, $p = 4.8\times10^{-6}$. Post hoc comparison to cue reaction: 500 ms, $p=1.9\times10^{-11}$, 1 s, $p=8.4\times10^{-11}$,
139 1.5 s, p=0.359, 2 s, p=0.005). This dependence on a short interval delay is consistent with the
140 temporal characteristics of canonical cerebellar-dependent sensorimotor associative learning[22].
141 To test whether animals adjust the timing or kinematics of their forelimb movement to
142 predict the timing of the visual cue, we measured lever kinematics during a subset of learning
143 sessions. Alignment of the lever trajectory to the onset of the cue revealed that animals altered
144 the time of lever release, releasing the lever sooner in anticipation of the visual cue (Fig. 1I; 20%

145 rise time occurs 116 ± 18 ms earlier, p = $1.2x10^{-5}$, paired t-test). However, despite substantial
146 variability in the kinematics of release (Supp. Fig. 3), independent alignment of both press and
147 release demonstrated that there was no change in movement kinematics across learning
148 sessions (Fig 1I-J; First 1/3 of session 20-80% release rise time= 18.9 ± 0.6 ms, last 1/3 of session
149 = 19.3 ± 0.8 ms; p=0.513, paired t-test), indicating that mice release the lever sooner but with the
150 same kinematics after learning.

151 To test the necessity of the lobule simplex for this learning, we first locally applied lidocaine
152 in order to block spiking in cerebellar cortical neurons, including PCs. However, consistent with
153 the critical tonic inhibition PCs provide to the deep cerebellar nuclei, we observed significant motor
154 deficits including slowed movement, dramatically fewer initiated trials, and dystonic limb
155 contractions (not shown). Thus, this manipulation was not appropriate to define the necessity of
156 lobule simplex in our task.

157 To avoid significant impairment of motor output, we next used a pharmacological
158 manipulation to selectively disrupt excitatory synaptic transmission in lobule simplex without
159 abolishing the spontaneous pacemaking of PCs. For these experiments, we optimized
160 concentrations of the excitatory synaptic transmission blockers NBQX (300 μM), CPP (30 μM)
161 and MCPG (30 μM) to avoid visible impairment of motor output, and then tested this cocktail
162 during behavior. Following local drug application to lobule simplex (methods), mice retained the
163 ability to release the lever in response to the visual cue, maintaining stable kinematics across
164 sessions (Fig. 2A,B) that were not different from control sessions (Fig. 1I,J, and Supp. Fig. 3;
165 Press: control range = 28.97 ± 2.5 ms, NBQX range = 25.33 ± 1.9 ms, p=0.2612; Release: control
166 range = 6.16 ± 1.2 ms, NBQX range = 4.13 ± 1.06 ms, p=0.2215, unpaired t-test). These data
167 suggest that motor output was not significantly impaired as a result of this pharmacological
168 manipulation. However, despite stable movement kinematics, learning was severely impaired
169 when the cue was presented with a constant 500 ms delay (Fig 2A,C,D) (NBQX ΔRT with 500 ms
170 cue delay = 48.8 ± 26.7, control ΔRT with 500 ms cue delay = 154.5 ± 13.6 ms, ΔRT with cue
171 reaction = 1.1 ± 9.3, unpaired t-test NBQX vs control 500 ms p=$4.6x10^{-4}$, unpaired t-test NBQX
172 vs control cue reaction p=0.05). Acute single unit PC recordings during drug application revealed
173 that this manipulation significantly reduced complex spike rates, consistent with a reduction in the
174 amplitude of postsynaptic glutamatergic currents produced by climbing fiber input (control 0.60 ±
175 0.07 Hz, NBQX/CPP/MCPG 0.27 ± 0.04 Hz, n = 9, p=$8.5x10^{-4}$, paired t-test, Supp. Fig. 4). We
176 also found a modest reduction in simple spiking, consistent with reducing excitatory synaptic input
177 from the mossy fibers and parallel fibers (control 66.8 ± 17.8 Hz, NBQX/CPP/MCPG 45.9 ± 13.0
178 Hz, n = 8, n = 9, p=0.36, paired t-test). Hence, these data support that hypothesis that synaptic

179 transmission in lobule simplex is necessary for predictive sensorimotor learning in our task, thus
180 implicating known mechanisms of cerebellar cortical learning.
181
182 **Complex spiking is not driven by motor errors in a voluntary motor learning task**
183 Because climbing fibers provide key instructional signals for cerebellar learning, we next
184 sought to test what information is conveyed by the olivary system in this behavior. Thus, we
185 imaged climbing fiber evoked calcium signals in mice engaged in the cue reaction condition. In
186 this regime, all sensorimotor signals are in place to drive learned, predictively timed forelimb
187 movements, but no learning can occur due to the variable cue timing (Fig. 1G,H). Hence, we can
188 test what task features drive complex spiking in a stable regime. We began by using a single
189 photon microscope to image populations of PCs virally expressing GCaMP6f (methods). Image
190 segmentation in a subset of experiments with the most superficial GCaMP expression revealed
191 structures consistent in size and shape with PC dendrites in cross section (Supp. Fig. 5). Calcium
192 transients in these structures occurred at 0.5 $\pm$ 0.01 Hz, consistent with the baseline rate of
193 complex spiking we measured with single unit electrophysiology (Supp. Fig. 5). These results are
194 also consistent with several *in vivo* calcium imaging studies using a variety of GCaMP variants
195 showing that PC responses are dominated by the large dendritic calcium transients produced by
196 climbing fiber driven complex spikes[15-18, 23-28].
197 We next identified regions of interest, defined by the expression pattern of GCaMP in each
198 animal, that were restricted to the region within lobule simplex capable of driving ipsilateral
199 forelimb movements (methods). Consistent with the role of this region in the control of forelimb
200 movements, we observed task modulated PC calcium transients associated with the timing of
201 lever press and release, with the largest modulation at the time of lever release (Fig. 3A-C).
202 Surprisingly, when we segregated trials according to outcome, we observed significantly larger
203 calcium transients associated with lever releases when animals correctly released the lever in
204 response to the visual cue as compared to trials where lever release occurred prior to the cue
205 (Correct = 0.156 $\pm$ 0.023 $\Delta F/F$; Early = 0.092 $\pm$ 0.018 $\Delta F/F$, n=17 sessions, 10 animals, $p=4.60\times10^{-}$
206 ^{5}, paired t-test). These enhanced responses were distributed widely across dorsal, superficial
207 lobule simplex, and were consistent across sessions and animals (Fig. 3D). The same pattern of
208 enhanced complex spiking on correctly timed lever releases was observed in the cue prediction
209 condition, and was maintained across learning sessions, as measured by single unit PC
210 electrophysiological recordings (Supp. Fig. 6). Thus, in this motor task, our data suggest that
211 complex spikes occur preferentially in response to correctly timed movements, and not motor
212 errors.
213 There are many differences between the correct and early release trials that could
214 contribute to the observed outcome-dependent difference in complex spiking. One possible

215 difference between trial types could be the kinematics of the forelimb movement. Hence, in a
216 subset of our experiments, we measured movement kinematics by comparing lever trajectories
217 on correct and early release trials (Fig. 4A-B). These data revealed closely matched movement
218 kinematics between correct and early lever release trials (Press: correct = 26.8 $\pm$ 1.6 ms, early =
219 25.1 $\pm$ 1.3 ms; Release: correct = 18.9 $\pm$ 0.8 ms, early: 22.1 $\pm$ 1.5 ms, n=14 sessions).
220 Another difference between correctly timed and early lever releases is that reward is only
221 delivered on correct trials, and this results in extended licking. Indeed, we find that lick rates were
222 significantly higher and prolonged on correct trials (Fig. 4C; correct = 10.5 $\pm$ 0.7 Hz, early = 1.5 $\pm$
223 0.4 Hz, $p=3.74\times10^{-9}$, paired t-test, n=9 animals, 15 sessions). Moreover, in some recording
224 sessions we observed a late, sustained calcium transient that occurred during licking (Fig. 4D).
225 However, we found no correlation between the mean early, peak calcium transients and mean
226 lick rates across trial types (Fig. 4E,F; Correct $R^2=0.182$, p=0.11; Early $R^2=5.97\times10^{-5}$, p=0.98) or
227 within sessions across trials of each type (Fig. 4G; Correct ρ = -0.002 $\pm$ 0.028, p=0.93; Early
228 $\rho = 0.054 \pm 0.113$, p=0.65, one sample t-test; Supp. Fig. 7D; Correct ρ = 0.0053 $\pm$ 0.0019,
229 p=0.544; Early $\rho = 0.0912 \pm 0.0048$, p=0.428, n=447 dendrites, one sample t-test). Thus, we
230 conclude that the enhanced responses as measured by the early peak calcium transient on
231 correctly timed lever releases are not due to differences in forelimb movement kinematics or
232 licking (Figure 4 and Supp. Fig. 7), but are instead linked to the context of the movement.
233
234 **Behavioral context determines the probability and synchrony of complex spiking**
235 To investigate the dynamics of complex spiking at the single cell level, we used video-rate
236 two-photon microscopy to image the dendrites of PCs during behavior. Using this approach, we
237 isolated the dendrites of individual PCs[24] (Fig. 5, Supp. Figs. 5, 8), and measured both
238 spontaneous and task-evoked calcium transients. As with the single photon imaging experiments,
239 spontaneous calcium transients measured during inter-trial intervals occurred at a rate of 0.61 $\pm$
240 0.01 Hz, consistent with our electrophysiological measurements of spontaneous complex spiking
241 (Supp. Fig. 5E,F). The two-photon data also replicated the main finding that the mean calcium
242 transients were significantly larger on correct release trials within individual PC dendrites (Correct
243 = 0.101 $\pm$ 0.004 $\Delta F/F$; Early = 0.035 $\pm$ 0.002 $\Delta F/F$, n=1146 dendrites, $p=9.79^{-76}$, paired t-test) (Fig.
244 5A,B). Moreover, lever releases that were rewarded but occurred too fast to be responses to the
245 visual cue (reaction times less than 200 ms) produced calcium transients that were significantly
246 smaller than those produced by correct lever release trials ('Too fast' 0.029 $\pm$ 0.002 $\Delta F/F$, $p=3.91^{-}$
247 ^{104}, paired t-test) and not significantly different from responses on early release trials (p=0.086).
248 Hence, these data support the analysis in Figure 4 that the enhanced complex spiking on correct
249 trials is not due to licking or reward per se.

250 In addition to larger mean responses across trials, population level analysis revealed that
251 more PCs were driven on correct release trials (Fig 5C). Of the total population of PCs that
252 responded to any lever press or release (1146 of 1302), most (88%) PCs exhibited complex
253 spikes on correct release trials, whereas less than half (41%) responded during early lever
254 releases (Fig. 5D, *top*). Approximately half (48%) of PCs exhibited complex spikes in response
255 to lever press (Fig. 5D, *bottom*). The increased number of active dendrites on correct trials is
256 unlikely to be a thresholding artifact, since there was no significant difference in the average
257 response amplitude of correct-only and correct+early responsive dendrites to correct trials
258 (Correct only 0.112 $\pm$ 0.006 $\Delta F/F$, n=578; Correct + Early 0.119 $\pm$ 0.005 $\Delta F/F$, n=457 dendrites,
259 p=0.44 unpaired t-test). These data also indicate that the measured increase in number of active
260 dendrites is not due to contamination of fluorescent signals from neighboring dendrites. Hence,
261 these single dendrite measurements explain our single photon results by demonstrating that both
262 more PCs exhibit complex spikes on correct trials, and those dendrites that exhibit complex spikes
263 in response to both trial types have larger mean calcium transients on correct trials.
264 The difference in the average release-evoked response on correct versus early trials may
265 be due to a difference in the amplitude of the calcium transients on each trial. For instance,
266 complex spikes are not "all-or-none" events[29], and the number of spikelets can vary from event to
267 event[30-32], altering the size of the evoked calcium transient[33]. Thus, we extracted single trial
268 events associated with lever releases across trial types, and compared these with each other and
269 to the spontaneous calcium transients. However, this analysis revealed no significant difference
270 between the amplitude of calcium transients evoked on single trials in response to either correct
271 or incorrect lever releases (Correct 0.266 $\pm$ 0.004 $\Delta F/F$ n=19,550 events, Early 0.263$\pm$ 0.004 $\Delta F/F$
272 n=9,167 events), and between movement-evoked and spontaneous activity (Spontaneous 0.272
273 $\pm$ 0.004 $\Delta F/F$ n=286,964 events) (p=0.17, one-way ANOVA) (Fig. 5E). Thus, if there are variable
274 numbers of evoked spikelets across trials, such differences are not systematically correlated with
275 either trial outcome or task engagement. Moreover, the equivalent amplitude of lever-evoked and
276 spontaneous events suggests that the majority of the signal measured in response to lever
277 release is from calcium influx due to complex spiking. Indeed, the size and shape of our
278 segmented ROIs is consistent with several studies showing that complex spikes produce a
279 calcium signal throughout the entire PC dendrite[7, 9], whereas parallel fiber calcium signals are
280 much smaller and confined to isolated regions of spiny dendritic branchlets[34-37].
281 To assess how equivalent single event responses can produce larger mean responses on
282 correct trials, we generated a peristimulus time histogram of complex spike events for each trial
283 type aligned to the time of release (Fig. 6A). This analysis revealed a significantly enhanced
284 complex spike rate at the time of lever release for trials when movement was correctly timed (Fig.
285 6A,B; correct spike rate=2.04 ± 0.05 Hz, early spike rate= 1.33 ± 0.04 Hz, $p=8.14\times10^{-15}$, n=1146

286 dendrites, paired t-test). In addition, complex spiking on correct trials in single PC dendrites
287 occurred with shorter latency (Fig 6C; correct latency=35.86 ± 1.19 ms, early latency=46.49 ±
288 1.25 ms, $p=2.65x10^{-11}$, n=1146 dendrites, paired t-test) and less temporal jitter across trials (Fig
289 6D; correct jitter (S.D of latency) = 104.1 ± 2.2 ms S.D., early jitter 112.3 ± 2.0 ms S.D., p=0.007,
290 n=1146 dendrites, paired t-test). Notably, these measures of jitter are likely to be an overestimate
291 since our measure of event time is limited by our sampling interval (33 ms), and the true onset
292 might have occurred between samples. However, when accounting for the overall spontaneous
293 event rate of ~1 Hz, the 100 ms jitter of events on correct trials is comparatively precise.
294 The PSTH reveals that the increase in complex spiking occurs proximal to the lever
295 release. To test whether the increase in complex spiking is more closely associated with the lever
296 release or the visual cue, we compared the temporal jitter of spike times on correct trials when
297 aligned to each of these events. This analysis revealed a significantly lower temporal jitter when
298 the spikes were aligned to lever release as measured either with imaging (Fig 6F; release jitter:
299 104.1 ± 2.2 ms S.D., visual cue jitter 119.5 ± 4.3 ms S.D., $p=6.2x10^{-5}$, n = 1146 dendrites; paired
300 t-test) or at higher temporal resolution with electrophysiology (Supp. Fig. 6F; release jitter: 0.118
301 ± 0.002 ms S.D., visual cue jitter 0.132 ± 0.003 ms S.D., n = 40 cells; $p=7.8x10^{-9}$; paired t-test).
302 Notably, the closer association between spiking and the lever release was maintained across
303 learning in cue prediction sessions, even as lever releases became more closely matched with
304 the timing of the visual cue (Supp. Fig. 6E-F). In addition, we find that the latency to peak event
305 rate is strongly correlated with reaction time when the events are aligned to visual cue (Fig 6G;
306 r=0.90, $p=8.56x10^{-12}$, Pearson's correlation), but not when aligned to lever release (r=-0.28,
307 p=0.13). These results further suggest a closer association between lever release and complex
308 spiking than for the visual cue and complex spiking.
309 The narrower PSTH on correct release trials is also consistent with the possibility of
310 enhanced synchrony on the time scale of ~100 milliseconds at the population level. Indeed, we
311 find enhanced population synchrony across dendrites (Fig 6E; correct jitter (S.D of latency) = 92.5
312 ± 3.1 ms S.D., early jitter 100.5 ± 3.1 ms S.D., p=0.003, n=1146 dendrites, paired t-test).
313 However, in many experiments, we observed no such increase in population synchrony on correct
314 trials (16 out of 30 sessions do not have significantly elevated synchrony on correct trials, open
315 circles, p>0.05 for each session). We thus considered the possibility that enhanced synchrony
316 was location specific, and might obey spatial structure that was not well demarcated at the scale
317 of the field of view in our two-photon experiments.
318
319 **Context determines correlated population activity at the mesoscale level**
320 To investigate whether correlated complex spiking was spatially organized, we returned
321 to single photon imaging and analyzed experiments that exhibited widespread GCaMP

322 expression across superficial lobule simplex (n=5 animals, 7 sessions). Using an unsupervised,
323 iterative pixel-clustering approach[26] (methods), we first assessed correlations between pixels
324 across all trials (Fig. 7A). Despite non-uniform, unpatterned GCaMP expression, this analysis
325 revealed spatial patterns of correlated activity that were organized across parasagittal bands
326 oriented in the rostro-caudal axis. These bands were 221 $\pm$ 15 μm wide on average across 39
327 measured zones, consistent with previous anatomical and physiological measurements of
328 cerebellar microzones[38, 39]. Hence, these data support the longstanding hypothesis that the
329 anatomical pattern of climbing fiber projections into the cerebellar cortex establishes functionally
330 distinct parasagittal processing modules.
331 To test how complex spiking is modulated during behavior within and across parasagittal
332 zones, we divided trials according to outcome and analyzed brief epochs surrounding the time of
333 lever release (Fig. 7B). While this analysis lacks the fine temporal resolution of the two-photon
334 event based analysis in Figure 6, it nonetheless revealed that activity amongst pixels within a
335 zone exhibited higher correlations for most zones on correct lever release trials as compared to
336 early release trials ($r_{correct}$ = 0.77 $\pm$ 0.01, r_{early} = 0.69 ± 0.017, p = 1.60x10^{-5}, n=39 clusters, paired
337 t-test) (Fig. 7C). Because higher spike rates can cause larger correlations, we tested whether
338 the higher complex spike rates on correct trials could account for the higher correlations. While
339 increased complex spiking did produce larger correlations, early release trials still had weaker
340 correlations than correct release trials across equivalent activity levels as assessed by linear fits
341 to bootstrapped distributions paired from each trial type (methods) (Fig. 7D). Hence, the
342 enhanced correlations on correct trials are not an artifact of enhanced complex spike rates on
343 correct trials. We also found enhanced correlations between neighboring and non-neighboring
344 zones on correct lever release trials (Fig. 7E,F) (Correct $r_{neighboring}$ = 0.69 $\pm$ 0.03, n=31 cluster
345 pairs, p=0.004 vs early, Correct $r_{non\text{-}neighboring}$ = 0.65 $\pm$ 0.03, n=50 cluster pairs, p=6.2x10^{-12} vs
346 early, paired t-test). However, these cross-zone correlations were significantly lower on average
347 than those within zones (within zone vs neighboring, p=0.004; within zone vs. non-neighboring
348 p=3.4x10^{-4}, unpaired t-test). Hence, these data reveal a precise spatial organization of climbing
349 fiber activity, with highly correlated complex spiking within parasagittal zones that is task specific,
350 differing for movements with the same kinematics depending on behavioral context.
351
352 **Complex spiking signals learned sensorimotor predictions**
353 Our data suggest that complex spiking does not signal motor errors in this behavioral
354 paradigm. Instead, our results are consistent with the possibility that the climbing fibers either 1)
355 instruct a different type of supervised learning rule based on correctly timed motor output, or 2)
356 provide a reinforcement learning signal, such as a temporal-difference (TD) signal of the type
357 recently identified for climbing fibers during conditioned eyeblink learning[40]. While the

instructional signals for supervised learning encode specific outcomes, those for reinforcement learning are driven by prediction errors. Thus, while a reinforcement learning signal should occur to any unexpected outcome (e.g. unexpected reward) or event that predicts task outcome, a supervised signal based on correct movements should only occur for correctly timed arm movements in our task. We hence began by testing whether climbing fibers can be driven by unexpected reward.

Surprisingly, when reward was delivered unexpectedly during the intertrial interval, we observed robust climbing fiber responses of similar amplitude to those driven by correctly timed lever releases (Figure 8A, Supp. Fig. 9). Because we have already demonstrated that the increase in climbing fiber activity is not driven by licking or reward (Figs. 4, 5B, Supp. Figs. 7,9), we interpret the increase in complex spiking in response to an unexpected reward as evidence of a prediction error. We hence conclude that climbing fibers do not specifically represent correctly timed movement per se, but may instead provide input consistent with a reinforcement learning rule.

To further test whether climbing fiber activity in our task is consistent with a reinforcement learning signal, we next tested whether the climbing fibers respond to other task features that predict task outcome (reward delivery). Thus, we took advantage of the temporal structure of the task, wherein the probability of cue appearance, and thus reward delivery, increases with lever hold time (i.e. the hazard function is not flat). We specifically tested whether complex spiking depends on lever hold time for correct and early lever releases.

We find that while complex spiking is independent of lever hold time for correctly timed movements (correct- 1P: $\rho = -0.07$, p=0.76, n=17 sessions ; 2P: $\rho = -0.01$, p=0.98 n=30 sessions; Fig. 8 B, Supp. Fig.10), there is a strong positive relationship between lever hold time and complex spiking for early lever releases across both single and multiphoton imaging sessions (early- 1P: $\rho = 0.91$, $p<1.0\times10^{-16}$, n=17 sessions; 2P: $\rho = 0.90$, $p=4.58\times10^{-6}$, n=30 sessions; Fig. 8 A,B). The elevated complex spiking associated with longer lever hold times is due to both an increase in spiking at the time of lever release (Window 1: short duration early $\Delta F/F = 0.03 \pm 9.55\times10^{-4}$, long duration early $\Delta F/F = 0.04 \pm 0.00$, $p=3.84\times10^{-10}$, n=1146 dendrites, paired t-test; Figure 8C), and an additional late response not present on short duration early release trials (Window 2: short duration early $\Delta F/F = 0.04 \pm 0.00$, long duration early $\Delta F/F = 0.07 \pm 0.00$, $p=1.33\times10^{-25}$; Figure 8C). The late response occurred on single trials and within individual dendrites, indicating that it was not generated by a diversity of response timings across trials or by a separate population of PC dendrites (Fig. 8 D). In addition, the late response occurred approximately 200 ms after lever release when reward delivery was no longer possible and lick rates began to decrease (Fig 8 H,I). This provides another important piece of evidence that increases in licking cannot explain the observed increases in complex spiking. Instead, this result reveals that licking is tightly linked to

394 the animals' expectation: when the animal no longer expects reward, lick rates decrease. In the
395 same manner, because spontaneous licks can reflect an expectation of possible reward, it is not
396 surprising that spontaneous licks are sometimes associated with increases in complex spiking
397 (Supp. Fig. 7).

398 Each of these results are consistent with a reinforcement learning rule based on prediction
399 error, where complex spiking increases in response to both learned task events that predict
400 reward and unexpected outcomes (in this case, the lack of reward following long duration early
401 releases). In this model, an initial prediction accompanies lever release that depends primarily on
402 cue presentation. Thus, complex spiking in response to correct releases is significantly stronger
403 than on early releases, even for long duration holds (Window 1: long duration correct $\Delta F/F = 0.07$
404 $\pm$ 0.00, long duration early $\Delta F/F = 0.04 \pm 0.00$, $p = 3.16 \times 10^{-7}$, n=1146 dendrites, paired t-test).
405 However, while the visually driven lever release provides the strongest prediction of trial outcome,
406 trial duration also contributes to expectation according to the task structure. In the case that initial
407 expectation is unmet, the climbing fibers also signal this unexpected outcome through an increase
408 in spiking. Notably, this latter result argues that climbing fibers encode an unsigned prediction
409 error, in which there is an increase in spiking regardless of the direction of the prediction error.

410 To further test this model, we performed a second set of experiments to probe the role of
411 violated expectations in driving complex spiking. In these experiments, we omitted reward
412 delivery on 20% of correctly timed lever releases (Fig. 8 J-N). Consistent with the cue appearance
413 establishing expectation at the time of lever release, both rewarded and omission trials resulted
414 in calcium transients that were nearly equivalent at the time of lever release (Window 1: rewarded
415 = 0.07± 0.01, omission = 0.07 ± 0.01; p=0.04, n=81 dendrites, paired t-test; Figure 8L). However,
416 omission trials resulted in an additional, late response at the time when reward delivery was no
417 longer possible and lick rates began to decrease (Window 2: rewarded = 0.06± 0.01, omission =
418 0.08 ± 0.01; $p=2.54 \times 10^{-9}$, n=81 dendrites, paired t-test; Figure 8M). The timing of this late
419 response was similar to the late response following long duration early releases, and was present
420 on single trials and within individual dendrites (Figure 8J,N). Hence, these experiments support
421 the hypothesis that climbing fibers can both signal and evaluate predictions about the likely
422 outcome of movements in a manner consistent with a reinforcement learning rule.
423

424 **Discussion**

425 We have established a sensorimotor association task that involves PCs near the dorsal
426 surface of lobule simplex. This behavior has several hallmarks of cerebellar learning, including a
427 dependence on short delay intervals for generating the learned sensorimotor association and the
428 requirement for excitatory synaptic transmission in the cerebellar cortex. In this behavior,
429 however, climbing fibers do not signal erroneous motor output as described by classical models

430 of supervised learning. Specifically, we demonstrate that climbing fiber driven complex spiking
431 occurs with higher probability, shorter latency, and less jitter when movement is correctly timed.
432 Our data support the hypothesis that these enhanced climbing fiber responses are related
433 to the predicted outcome of movement, which in this behavior constitutes delivery of a water
434 reward. Evidence supporting this model is threefold: First, the highest probability of complex
435 spiking occurs on correctly timed lever releases when the visual cue instructs behavior and thus
436 a high reward expectation. Second, complex spiking is modulated by the temporal features of the
437 task that dictate expectation. Specifically, complex spiking in response to lever release increases
438 with increasing hold duration, matching the increased likelihood of reward as trial length
439 increases. Third, complex spiking is also driven when the expectation of reward is violated: when
440 the reward is omitted on correctly executed movements, not provided on longer hold duration
441 early releases when a correct outcome of lever release is probable, or unexpectedly presented
442 during the inter-trial interval. Together, these experiments suggest that climbing fibers carry
443 instructional signals that both predict and evaluate the expected outcome of movement in a
444 manner consistent with a reinforcement learning rule. Such responses are also consistent with
445 the known role of cerebellar circuits in generating predictive motor output, and we suggest that
446 they could thus provide a substrate for generating and testing the type forward models that have
447 long been hypothesized to govern cerebellar processing.
448 The climbing fiber activity observed in response to violated expectations has some
449 similarities to the motor error signals seen in classic cerebellar behaviors. However, in our
450 behavioral paradigm, we emphasize that these climbing fiber responses do not reflect motor
451 errors: the movements on trials in which rewards are omitted are identical to those in which
452 rewards are earned. Thus, these results indicate that the climbing fibers can respond differentially
453 to the very same movement according to its expected outcome. These context-specific climbing
454 fiber responses may be due to aspects of our task design. The behavior described here differs
455 from most cerebellar dependent learning regimes in that the movement requiring modification
456 (lever release) is not directly related to an unconditioned stimulus (reward) or response (licking).
457 As a consequence, the cerebellum cannot harness sensorimotor input from hardwired pathways
458 to enable learned changes in motor output. Instead, the necessary forward model must define
459 and evaluate the relationship between a neutral visual stimulus, a forelimb movement, and
460 reward.
461 It remains unclear whether the climbing fiber activity that enables such a forward model is
462 generated at the level of the olive, or if it is inherited from upstream brain regions such as the
463 neocortex, colliculus, or elsewhere. However, evidence suggests that the olive may have access
464 to different information depending on task requirements. Anatomical and physiological work in the
465 rodent has demonstrated that the pathway from the forelimb region of motor cortex to the IO is

466 independent of the pathway providing ascending sensorimotor input to the olive from the
467 periphery[41]. Such data argue that the olive has access to unique information in tasks that involve
468 a descending motor command, and further suggest that the olive may have access to diverse
469 cortical computations. Indeed, the presence of abstract task timing information in the activity of
470 the climbing fibers suggests that the olive has access to higher-order signals. In support of this
471 view, evidence from a different forelimb movement task in non-human primates that also requires
472 an abstract sensorimotor association has shown similar climbing fiber responses[42]. Specifically,
473 this study demonstrated that complex spikes can signal both the predicted destination of reaching
474 as well as deviations from the expected destination.

475 Importantly, the climbing fiber activity patterns described here are appropriate to drive
476 motor learning under conditions that require flexible sensorimotor associations. Specifically, the
477 higher probability complex spiking and enhanced correlations at the population level are both
478 context dependent and spatio-temporally organized. At the population level, our single photon
479 imaging of cerebellar complex spiking has revealed correlated activity within parasagittal bands
480 of approximately 200 μm, likely corresponding to "microzones"[16, 26, 39, 43-47]. Because PCs across
481 microzones can respond to different sensorimotor input, and have different spiking[48] and
482 synaptic[49] properties, these zones are thought to constitute discrete computational units in the
483 cerebellum. Recent measurements have revealed that complex spiking in microzones can
484 become more synchronous during both motor output[18] and sensory input[15, 16, 27]. Our population
485 imaging results provide a fundamental extension to this idea by demonstrating that correlated
486 complex spiking within parasagittal zones is not simply enhanced by sensorimotor input, but
487 rather can be enhanced for the same action according to behavioral context. Precisely timed
488 spiking across a large population of nearby PCs that receive common parallel fiber input and
489 converge to the same DCN neurons would provide an ideal substrate to maximize the impact of
490 plasticity. However, other circuits could also play a role in learning. In particular, complex spiking
491 can robustly inhibit nuclear neurons[50, 51], and enhanced climbing fiber synchrony would magnify
492 this effect via convergence of simultaneously active PC axons in the DCN[52]. Because
493 synchronous inhibition has been shown to play a key role in synaptic plasticity at nuclear neuron
494 synapses[53, 54], correlated complex spiking across populations of nearby PCs could place the DCN
495 as the central site of learning under such conditions[55]. In either case, we note that the climbing
496 fiber responses following correct lever releases are well-timed to promote learning in the cue
497 prediction condition by instructing movements that more closely approximate earliest time of
498 reward delivery.

499 Finally, it is notable that ours are not the first results to suggest alternate learning rules
500 instructed by climbing fiber activity. Recently, conditioned eyeblink learning data has pointed
501 toward climbing fibers implementing temporal difference (TD) reinforcement learning rule by

signaling sensory prediction errors in order to instruct motor learning[40]. Because we do not observe evidence of negative prediction errors on reward omission trials or long duration early release trials, our results are incompatible with this model as strictly interpreted. Instead, our data show some similarities with the type of unsigned prediction signals observed in serotonergic[56] and other neurons[57, 58] that have been also thought to enable associations between unexpected outcomes and novel cues[59]. Evidence for both models can often be found in neural activity within the same brain region, and it has been suggested that TD and unsigned prediction mechanisms may in fact be linked, and act together to promote learning[60]. Hence, as has been done in other brain regions, it will be necessary to systematically vary task parameters such as the valence of instructional stimuli and the requirements for learned associations in order to resolve how the cerebellum implements discrete learning rules according to task demands. For the present, the results described here provide an important new demonstration that complex spiking can signal learned, task specific information necessary for flexible control of complex motor behaviors in a manner that does not depend exclusively on motor errors.

Author Contributions

WH, ES, AM, MJ, and CH designed experiments, WH, ES, AM, BT, MAH, and MJ conducted experiments, WH, ES, ZX, BT, AM, MJ, and CH analyzed data, and CH wrote the manuscript.

Figure Legends

Figure 1. Cerebellar sensorimotor task for head-fixed mice. Ai) Confocal image of a sagittal section from PCP2-Cre x Arch mouse showing expression of the inhibitory opsin Arch in PCs at low (left) and high (right) resolution. ML; molecular layer, PCL; Purkinje cell layer, GCL; granule cell layer. Aii) Schematics of a cranial window implanted over lobule simplex (left) and configuration for optogenetic stimulation (right). Bi) *Left*, representative single unit recording of PC simple spike raster (top) and spike rate histogram (bottom) aligned to onset of Arch activation. *Right*, Location of the stimulation sites that evoked ipsilateral forelimb movements (green). Bii) Average normalized firing rates from superficial (top) or deep (bottom) PCs at low (left) or high (right) stimulation powers (n=5 mice; 10-20 mW – superficial: n=6 cells; deep: n=5 cells; 30-50 mW – superficial: n=10 cells; deep: n=4 cells). Note that the lower powers used to map motor responses were only sufficient to strongly suppress neurons above 500 μm. C) Schematic of

538 configuration of behavioral task. Head-fixed mice were trained to release a lever in response to a
539 visual cue, with reward delivered immediately upon correctly timed movement. D) Schematic of
540 trial structure. The delay between lever press and release cue was either randomized (cue
541 reaction) or constant (cue prediction) from trial to trial. E) Average reaction time (from cue onset)
542 as a function of trial number for an example cue reaction session. Each point is the average of 5
543 trials. F) Same as E, for a cue prediction session. G) Summary of reaction times for all cue
544 prediction sessions with a 0.5 s cue delay (gray; n=44 sessions, 10 mice) and all cue reaction
545 sessions (black; n=26 sessions, 7 mice). Error bars are ±SEM across sessions. H) Average
546 change in reaction time from the beginning to the end of cue prediction and reaction sessions
547 (methods). I) *Top*, average lever kinematic traces from an example 0.5 s cue prediction session
548 aligned to the cue show that lever releases occur sooner in the last 1/3 of trials (black) as
549 compared to the first 1/3 of trials (gray). Shaded area is ±SEM across trials. *Bottom,* same
550 example session as above aligned separately to press and release showing no difference in
551 kinematics from beginning (gray) to end (black) of the session. J) Summary of average lever
552 release times (20-80% rise time) across sessions (n=15 sessions, 4 mice)
553
554 **Figure 2**. Learning requires synaptic transmission in lobule simplex. A) Average lever kinematic
555 traces from an example 0.5 s cue prediction session after application of NBQX (300 μM), CPP
556 (30 μM) and MCPG (30 μM). *Top*, traces aligned separately to press and release showing no
557 difference in kinematics from beginning (blue, first 1/3 of trials) to end (black, last 1/3 of trials) of
558 the session. *Bottom*, traces aligned to the cue show that lever releases do not occur sooner in
559 the last 1/3 of trials (black) as compared to the first 1/3 of trials (blue). Shaded area is ±SEM
560 across trials. B) Summary of average lever release times (20-80% rise time) across NBQX 0.5s
561 cue prediction sessions (n=10 sessions, 6 mice). C) Summary of all 0.5 s cue prediction sessions
562 where NBQX (n=14) CPP (n=14) and MCPG (n=8) were applied locally to LS (blue; n=6 mice)
563 compared to summary of cue reaction sessions (black; replotted from Fig 1G). D) Average
564 change in reaction time from the beginning to the end of NBQX 0.5s cue prediction sessions (blue;
565 n=10 sessions, 6 mice) compared to cue prediction and reaction sessions (replotted from Fig. 1H)
566
567 **Figure 3.** Single photon imaging during cue reaction sessions. A) Example ΔF/F single trial
568 timecourses for a correctly timed lever release (left) and an early lever release (right). RW =
569 reward, delivered immediately on correct release. B) Field of view (images separated by 100 ms)
570 showing the average fractional change in fluorescence aligned to lever release for correct (top)
571 and early (bottom) trials from an example session (same session as example from A. C) Calcium
572 transient timecourses averaged across trials from the experiment in A,B) for correct (black) and
573 early trials (red). Error bars are ±SEM across trials. D) Summary of the average peak calcium

574 transients (measured on single trial basis, methods) for all correct and early trials across sessions
575 (n=10 animals, 17 sessions). Colors represent different animals, and each point represents an
576 imaging session. Note that all points lie below the diagonal. *Inset*, schematic of ROIs for all
577 sessions. Outline color corresponds to mouse from scatter plot, and fill color indicates imaging
578 depth identified by post-hoc histology.
579
580 **Figure 4**. Lever dynamics and licking do not explain differences in complex spiking across trial
581 types. A) Average lever kinematics from a representative cue reaction session for correct (black)
582 and early (red) trials aligned to threshold crossing for both press and release. B) Summary of rise
583 times for press (left) and release (right) on correct and early trials across sessions (n=14 sessions,
584 3 mice). C) Average timecourse of licking for correct (top) and early (bottom) release trials across
585 sessions (n=15 sessions, 9 mice). Error bars are ±SEM across sessions. D) Two example
586 sessions illustrating the relationship between release-evoked calcium transients (black and red
587 lines) and licking (blue bars) for correct (left) and early (right) release trials. E) Summary of the
588 relationship between lick rates and the magnitude of fluorescent transients for correct (black) and
589 early (red) release trials (n= 15 sessions, 9 mice). Error bars are ±SEM across trials. F) Summary
590 of the mean ratio of early and correct trial-evoked peak calcium transient and lick rates for the
591 same sessions in E. G) Summary of the Spearman's correlation (ρ) between lick rate and peak
592 $\Delta F/F$ on correct (black) and early (red) lever releases across trials for each session (n=8 sessions,
593 7 animals). Filled circles are mean and SEM across sessions.
594
595 **Figure 5**. Complex spiking produces larger mean response in individual dendrites and enhanced
596 population responses when movement is correctly timed. A) *Left*, average GCaMP fluorescence
597 from an example 2-photon imaging session (30 Hz acquisition rate). Scale bar = 100 μm. *Middle*,
598 pixel mask of individual PC dendrites extracted from the same session. Right, average calcium
599 responses measured from the highlighted dendrite segregated by trial event. Dotted line
600 represents time of lever press (blue) or lever release (correct: black; early: red). Shaded area is
601 ±SEM across trials. B) Left, average timecourse of calcium response for all significantly
602 responsive dendrites aligned to lever press (blue), or release (correct releases (black), early
603 releases (red), and too-fast releases (green) that occurred < 200 ms following the visual cue;
604 n=17 animals, 30 sessions, 1146 dendrites). Shaded area is ±SEM across dendrites. *Middle*,
605 summary scatter plot comparing the average peak amplitude of the calcium transient for each
606 significantly responsive PC dendrite (gray) and the average of all dendrites (red) for correct and
607 early release trials. *Right*, same as middle for correct and too fast release trials. C) Pixel masks
608 of dendrites significantly responsive to lever release on correct trials, lever release on early trials,
609 and lever press for the example session in A. Color map represents average $\Delta F/F$. D) Summary

610 across experiments of the fraction of dendrites responsive to correct lever releases vs early
611 releases (top, left), to only correct or only early releases (top, right), to lever press vs release
612 (bottom, left), and only to press or release (bottom, right). E) *Left,* average amplitude of correct
613 and early release-evoked calcium events across all dendrites normalized to the amplitude of
614 spontaneous calcium events. *Right,* mean spontaneous (gray) and correct (black) and early (red)
615 release lever-evoked calcium events across all responsive dendrites Error bars are ±SEM across
616 cells.
617
618 **Figure 6**. Complex spiking occurs with higher peak rates and greater synchrony when movements
619 are correctly timed. A) Peri-release time histogram of calcium events on correct (black) and early
620 (red) release trials (n=17 animals, 30 sessions, 1146 dendrites). Bin width = 33 ms. Shaded area
621 is ±SEM across dendrites. B) Summary of average event rate for correct and early releases
622 across sessions. Error bars are ±SEM across dendrites. C) Same as B for average event latency
623 relative to release. D) Summary of average standard deviation (S.D.) across events within single
624 dendrites across trials. Error bars are ±SEM across dendrites. E) Same as D for measurement of
625 S.D. across dendrites within each experiment. Open circles are statistically significant for reduced
626 correct trial jitter across dendrites. Error bars are ±SEM across trials. F) Summary of the average
627 S.D. of spike times when aligned to either lever release or visual cue across sessions. Error bars
628 are ±SEM across dendrites. G) Summary of the average latency of the spike times relative to cue
629 (gray circles) or lever release (black circles) compared with the average session reaction time. X-
630 error bars are ±SEM across trials; Y-error bars are ±SEM across dendrites.
631
632 **Figure 7**. Complex spiking is correlated across parasagittal zones, with higher correlations on
633 correct lever releases. A) *Left*, Average GCaMP fluorescence for three example experiments.
634 ROIs from lobule simplex (white boxes) were selected for unsupervised clustering analysis (meta
635 K-means, methods). *Right*, voxels are colored according to cluster identity for each example
636 experiment. M=medial, R=rostral, C=caudal, L=lateral. Note the alignment of the clustered zones
637 along the rostro-caudal axis. B) Within cluster voxel-by-voxel correlations between correct and
638 early lever release trials from an example session in A (bottom) for each of the six identified
639 clusters (yellow). C) Summary of average correlation coefficient for all voxel pairs within an area
640 across experiments for correct and early release trials. (n=5 animals, 7 sessions, 39 clusters).
641 Colors denote clusters from the same session. Error bars are ±SEM across voxel pairs. D)
642 Summary of the relationship between peak ΔF/F and correlation coefficients for correct (black)
643 and early (red) trials. Lines are linear fits to each cluster. E) Same as C for pairs of voxels across
644 neighboring clusters. F) Same as C for pairs of voxels across non-neighboring clusters.
645

Figure 8. Complex spiking is modulated by learned sensorimotor predictions. A) Top, Average calcium transient in response to unexpected reward (green, aligned to first lick) and correct lever releases (black, aligned to release). Error is SEM across cells (n=120). Bottom, Average lick rate for unexpected reward and correct lever releases. Error is SEM across experiments (n=3). B) Summary of peak calcium transients in a 500 ms window at the time of release (methods) across all 2-photon experiments for correct (black) and early (red) release trials binned according to hold time (250ms bins). Linear fits were applied to data from each trial type (n=17 animals, 30 sessions). C) Mean timecourse of calcium transients for an example session divided according to early trials with hold durations of < 1.0s (red) and > 3.5s (dark red). Note the late, second response for long hold duration trials. D) Single trial example timecourses from an individual dendrite from the session in C). Gray bars represent analysis windows for subsequent plots E-G) Summary of peak calcium transients measured in the shaded windows from D for all dendrites (n=1146) according to lever hold time (E,F) and trial outcome (G). H) Mean calcium transient timecourses averaged across all dendrites on short and long hold early release trials. I) Mean lick rates for the subset of experiments where licking was measured in H (n= 6 animals, 10 sessions)). J) Example timecourses of mean calcium transients from a single session for correct (black), and reward omission (dark blue) trials. Note the late, second response on omission trials. K) Single trial example timecourses from an individual dendrite from the session in J. L-M) Summary of peak calcium transients measured in the shaded windows in K on correct and reward omission lever trials (n=81 dendrites, 3 animals, 3 sessions). N) Mean timecourses of calcium transients averaged across all dendrites for correct (black) and reward omission (dark blue) trials. Vertical bars represent the lick rate averaged across trials for all reward omission sessions.

Supplemental Figures

Figure 1. Mapping of motor output driven by Arch and electrical stimulation of superficial cerebellar cortex. A) Schematics of the results of Arch stimulation over a grid of sites in lobule simplex (Sim) and Crus I for all five mice. Colors denote outcome of stimulation. B) Same as A for three mice tested with electrical microstimulation.

Figure 2. Retention and extinguishment of learning for cue prediction regime. A) Average reaction times relative to cue for the first (left) and second (right) sessions where animals performed 0.5 s cue prediction on consecutive training days (n=17 sessions, 5 mice). Error bars are ±SEM across sessions. B) Same as A for 2 s cue prediction sessions (n=10 sessions, 6 mice). C) *Left,* example cumulative distributions of reaction times for cue reaction sessions immediately surrounding a cue prediction session (session 0). Trials from the cue prediction session include only the last 1/3 of the session when the animal was anticipating the cue timing.

682 *Right,* summary of distribution skewness across cue reaction sessions immediately surrounding
683 cue prediction sessions. D) Same as A for pairs of 0.5 s prediction sessions separated by 3 or
684 more cue reaction sessions (n=20 sessions, 10 mice).
685
686 **Figure 3**. Performance in the cue prediction condition in control and NBQX sessions. A-E)
687 Summary across experiments of average percent correct lever releases, baseline reaction time
688 from the visual cue, mean reaction time variance, mean duration to press, number of trials
689 performed, and the duration of behavioral sessions. n=44 0.5 s, n=9 1.0 s, n=6 1.5 s, n=30 2.0 s,
690 n=26 Δt, n=14 0.5 s NBQX. For each cue delay, the minimum and maximum (x,y) number of trials
691 performed in single sessions was: 0.5 s: (309, 700) 1 s: (252, 900) 1.5 s: (202, 775) 2 s:
692 (278,1185) Δt: (313, 772) 0.5 s NBQX: (227, 429). F_i) Individual (top) and average (bottom) lever
693 trajectories aligned to lever press (left) and release(right) segregated by duration into quartiles for
694 a representative 0.5 s cue prediction session. F_{ii}) Same as F_i for a representative 0.5 s cue
695 prediction session in NBQX. G) Summary of press (left) and release (right) quartiles across
696 experiments for control (top; n=15 sessions) and NBQX (bottom; n=14 sessions) experiments. H)
697 Summary of the ratio between press and release ranges (difference between 1st and 4th quartile)
698 for control (black) and NBQX (blue) experiments.
699
700 **Figure 4.** Pharmacological modulation of complex spiking in lobule simplex. A) Single unit
701 recordings during NBQX application to LS. Top, summary of complex spike rates in control and
702 after application of NBQX for individual cells (black; n=9 cells, 5 mice) and the average of all cells
703 (red). Error bars are $\pm$SEM across cells. Bottom, same as top for simple spike rates. Note that
704 NBQX strongly reduces complex but not simple spike rates. B) (top) Raw epifluorescence images
705 from parasagittal cerebellar sections showing fluorescein labeling after surface application to
706 lobule simplex *in vivo* (methods, 3 mice). (bottom) Pixel masks from the same images above.
707 Pixels were thresholded at 30% of maximum value to visualize and quantify fluorescein labeling.
708 C) Summary of mediolateral fluorescein spread across sections. (n=3 animals).
709
710 **Figure 5**. Segmentation of PC dendrites from imaging experiments. A) Example single photon
711 imaging field of view (left) is segmented to mask individual dendrites (right) used for subsequent
712 single cell analysis. Scale bar = 100 μm. B) Example timecourse of raw fluorescence (top) from
713 the circled dendrite in A showing individual calcium transients identified (gray circles) according
714 to peaks in the first derivative of the fluorescence trace (bottom). C) Same as A for an example
715 two photon field of view. Note that while PC somata are visible (round, top right), image
716 segmentation does not extract activity from these structures. Scale bar = 100 μm. D) Same as B
717 for the experiment in C. E) Top, example time course of a single unit PC recording from an

718 awake mouse illustrating detection of complex spikes (gray circles). Bottom, overlay of individual
719 simple (left) and complex (right) spike waveforms (gray) and the average waveform (black). F)
720 Summary of spike rates across all two photon dendrite imaging sessions (blue; n=1051 dendrites)
721 and acute single unit recordings (n=11 units).
722
723 **Figure 6**. Single unit PC recordings of complex spiking during the cue prediction condition. A)
724 Top, Schematic of the trial structure schematic, where a constant cue delay of 500ms was
725 imposed on each trial. Middle top, Average simple (SS, left) and complex (CS, right) spike
726 waveforms from an example single unit. Middle bottom, Histogram of SS firing rate aligned to
727 complex spike time revealing post-CS pause, confirming isolation of single PC. Bottom, raster of
728 single trial complex spikes and session PSTH aligned to lever release. B) Single trial voltage
729 traces (complex spikes- open blue circle) from the cell in A aligned to lever release (correct- black
730 circle; early- red circle). C) Expansion of 5 consecutive traces from B at time of lever release. D)
731 Mean normalized complex spike rate (methods) from single unit recordings (31 PCs, 8 mice)
732 aligned to lever release for correct (black) and early (red) trials during the cue prediction condition.
733 E). Mean normalized complex spike rates aligned to cue presentation for the first 1/3 of trials
734 (black) and the last 1/3 of trials (orange) across cue prediction sessions for correct (left) and early
735 (right) trials. F) Summary of the average S.D. of spike times when aligned to either lever release
736 or visual cue across sessions.
737
738 **Figure 7.** Differential complex spiking on correct and early release trials is not driven by motor
739 signals due to licking. A) Example imaging data from an inter-trial interval (ITI) showing a lick
740 responsive cell (top, dark blue) and a lick unresponsive cell (bottom, black) in the same field of
741 view. B) Averaged lick triggered calcium transients for the lick responsive cell (dark blue) and a
742 lick unresponsive cell (black) in A). C) Mean lick triggered calcium transient across all lick
743 responsive (dark blue) and lick unresponsive (black) cells. D) Summary of the Spearman's
744 correlation between lick rate and amplitude of the calcium transient in each frame across trials for
745 lick responsive (dark blue) and lick unresponsive cells (grey). Red points indicate the mean ±
746 SEM across dendrites (447 dendrites, 6 animals and 10 sessions) E) Summary comparing the
747 amplitude of calcium transients for lick responsive neurons only in response to either a single lick
748 (blue) or a lick bout (3 or more licks with ≤ 300 ms between licks; cyan). Note that additional
749 licking does not produce larger responses. F) Summary comparing the amplitude of calcium
750 transients on correct (black) and early (red) lever releases for lick unresponsive cells only. G)
751 Same as F, for lick responsive cells.
752

753 **Figure 8.** Example single trial and session average calcium transients from 2-photon imaging. A)
754 Example single trial data from an individual dendrite showing the normalized calcium transient
755 across an early release trial from before lever press to after the lever release. B) Same as A) but
756 for a correct trial, including the time of cue presentation. C) Mean calcium transients across trials
757 for the dendrite in A and B. D) Single trial example, aligned to lever release, showing all neurons
758 from the experiment illustrated in Fig. 5C on a correct trial over 1 second surrounding release.
759 Lever press is off scale. E) Same as D, but for an early release trial from the same imaging
760 session.
761
762 **Figure 9**. Unexpected reward drives complex spiking in lick unresponsive and responsive cells.
763 A-B) Top, Average calcium transient in response to unexpected reward (green, aligned to first
764 lick) and correct lever releases (black, aligned to release). Error is SEM across cells. Bottom,
765 Average lick rate for unexpected reward and correct lever releases. Error is SEM across
766 experiments (n=3). Lick responsiveness was defined according to significant responses in the
767 lick triggered averaged taken from the inter-trial interval (Supp. Fig. 7). C). Summary of peak
768 calcium transients in the same neurons for correct lever releases vs unexpected reward trials.
769 Note that responses are proportional, and response amplitude is determined by response
770 probability (Fig. 5,6).
771
772 **Figure 10**. Summary of peak calcium transients in a 500 ms window at the time of release
773 (methods) across all single photon experiments for correct (black) and early (red) release trials
774 binned according to hold time (250ms bins). Linear fits were applied to data from each trial type
775 (n=10 animals, 17 sessions).
776
777 **Figure 11.** Mice have full control over the lever trajectory. A) Individual (top) and average (bottom)
778 lever trajectories aligned to lever press (left) and release (right) for manual lever depression
779 followed by unperturbed gravity return. B) Summary of press (left) and release (right) quartiles
780 across experiments for manual lever experiments (n=4). Note the lack of variability across
781 quartiles. C) Summary scatterplot comparing 20-80% rise times of lever press and release for
782 experiments where the lever was controlled by mice (black) and manual press (green) D)
783 Summary comparison measuring the difference from the mean of the slowest release quartile and
784 the fastest release quartile for experiments where the lever was controlled by mice (black) and
785 manual press (green). Lever trajectories were sorted according to duration in a window from
786 200ms before threshold crossing to the time of a threshold crossing half way between the top and
787 bottom of the total lever displacement. The slowest and fastest 25 trials were extracted for
788 comparison, and their average rise time was normalized by subtracting that of the mean trajectory

789 of the whole session. These results show that mice produce movements both slower and faster
790 than the mean, indicating full control over the lever trajectory.
791
792 **Methods:**
793 Mice
794 All experimental procedures using animals were carried out with the approval of the Duke
795 University Animal Care and Use Committee. All experiments were performed during light cycle
796 using adult mice (>p60) of both sexes, randomly selected from breeding litters. All mice were
797 housed in a vivarium with normal light/dark cycles in cages with 1-5 mice. Imaging experiments
798 were performed using Tg(PCP2-Cre)3555Jdhu mice (Jackson Labs, 010536; n=12). Optogenetic
799 mapping experiments were conducted in PCP2-Cre animals crossed with Ai35(RCL-Arch/GFP)
800 (Jax 012735; n=5 mice). Single unit recordings during the cue prediction condition were
801 performed in wild type C57BL/6J mice (n= 8 mice). Additional behavioral experiments where
802 imaging was not performed were conducted in wild type C57BL/6J mice (n=18). We used two
803 exclusion criteria for animals in this study: (1) poor recovery or other health concerns following
804 surgical intervention or (2) missed virus injection, as determined by *in vivo* imaging and post-hoc
805 histological analysis.
806
807 Surgical Procedures
808 3-10 hours prior to surgery, animals received dexamethasone (3mg/kg) and ketoprofen (5mg/kg).
809 Surgical procedures were performed under anesthesia, using an initial dose of ketamine/xylazine
810 (50mg/kg and 5mg/kg) 5 minutes prior to surgery and sustained during surgery with 1.0-2.0%
811 isoflurane. Toe pinches and breathing were used to monitor anesthesia levels throughout
812 surgeries. Body temperature was maintained using a heating pad (TC-1000 CWE Inc.). Custom-
813 made titanium headplates (HE Parmer) were secured to the skull using Metabond (Parkell). For
814 imaging experiments, a 3mm diameter craniotomy was made over the lobule simplex
815 approximately 1.4mm lateral and 2.8mm posterior to lambda, and glass cover slips consisting of
816 two 3mm bonded to a 5mm coverslip (Warner Instruments No. 1) with index matched adhesive
817 (Norland No. 1) were secured in the craniotomy using Metabond. Buprenex (0.05mg/kg) and
818 cefazolin (50mg/kg) were administered following surgery twice a day for two days. Following a
819 minimum of 4 recovery days, animals were water deprived for 3 days, or until body weight
820 stabilized at 85% of initial weight, and were habituated to head restraint (3-5 days) prior to
821 behavioral training.
822 For imaging experiments, the glass cover slip was removed following behavioral training,
823 and mice were injected (WPI UMP3) with AAV1.CAG.Flex.GCaMP6f.WPRE.SV40 (UPenn vector
824 core, titer = 9.40×10^{12} or 7.60×10^{12}). 150 nL virus diluted 1:1-1:5 in ACSF was injected at a rate of

825 30nl/min and a depth of 150 μm at 1-3 sites in dorsal lobule simplex. Imaging was performed
826 beginning 14 days following injection.
827 For *in vivo* pharmacology experiments, a 3mm craniotomy was performed over lobule
828 simplex of headposted mice, and the dura mater was peeled back at the center of the craniotomy.
829 10uL of combined NBQX (300 μM) and CPP (30 μM) was applied into a well surrounding the
830 craniotomy on the surface of the cerebellum 20 minutes prior to behavioral training. In 8 of 14
831 experiments, MCPG (30 μM) was also included to block metabotropic glutamate receptors.
832 Because there no significant differences in performance across these two groups, all data were
833 pooled for analysis. During behavior, a second drug application of 10uL was administered 20 and
834 40 minutes into the task, and depending on the duration of training, a third dose was applied after
835 1 hour. Craniotomies were subsequently covered with silicone elastomer (WPI, Inc.) prior to
836 returning animals to their home cage. To quantify the spread of pharmacological agents in the
837 cerebellum, 10 μL of fluorescein dye (Sigma-Aldrich #F6377, 1mM in aCSF) was applied to the
838 craniotomy in 3 animals with the same method and timecourse as for drug applications. Following
839 standard histological processing and imaging (below), labeling was quantified by creating a binary
840 pixel mask thresholded at 30% of the maximum fluorescence value for each experiment. Dye
841 labeling was then measured using the area of these pixel masks (Supp. Fig. 4 B,C).
842
843 Behavior
844 During behavioral training, animals were head-fixed and placed in front of a computer monitor,
845 lever and reward delivery tube. Animals were trained to self-initiate trials by depressing the lever
846 using their right forepaw, and required to successfully hold the lever in the down position for
847 randomized intervals ranging between 500ms and 5 s on the cue reaction paradigm before
848 performing the cue prediction paradigm. For both paradigms, a high contrast hold cue was present
849 at all times, including the intertrial interval (ITI), and transitioned 90 degrees to the release cue on
850 each trial at the instructed time of release until the animal either released the lever or 1 second
851 had passed. Lever releases within one second of the release cue were rewarded immediately at
852 the time of lever release (0.01 M saccharine). Immediately following any lever release, a solenoid
853 was engaged to prevent lever press during the ITI. Following the ITI (3-6 s), the solenoid is
854 lowered, allowing the mouse to self-initiate a new trial. During training, a 1-3 second 'timeout'
855 was implement to punish early lever releases. No timeouts were used in fully trained animals for
856 imaging or behavior data collection sessions. For reward omission sessions, 20% of randomly
857 determined correct lever releases were unrewarded. Animals used for imaging experiments
858 performed the cue reaction condition with a mean peak percent correct of 79.7 ± 0.23% achieved
859 in 26 ± 2 training days. On imaging days animals performed a range of 150 to 580 trials per
860 session with a mean of 273.9 ±13.1 trials. Behavioral parameters including lever press, lever

861 release and licking were monitored using Mworks (http://mworks-project.org) and custom
862 software written in MATLAB (Mathworks). To assess the degree of lever control by the mice, the
863 dynamics of lever press and release trajectories were compared to lever presses initiated by the
864 experimenter where the lever was allowed to return to the rest position on its own (Supp. Fig. 11).
865 These results demonstrate that mice moved the lever both faster and slower than its intrinsic
866 kinematics, and thus had full control over its trajectory. Licking was measured with electrical
867 contact circuit. Inter-trial intervals ranged from 3 to 5 seconds.
868
869 Calcium Imaging
870 *Wide-field imaging*: Single photon imaging was performed using a customized microscope (Sutter
871 SOM) affixed with a 5x objective (Mitutoyo, 0.14NA) and CMOS camera (Qimaging, Rolera em-
872 c^2). Excitation (470 nm) was provided by an LED (ThorLabs, M470L3), and data were collected
873 through a green filter (520-536 nm band pass, Edmund Optics) at a frame rate of 10Hz, with a
874 field of view of 3.5x3.5mm at 1002x1004 pixels.
875
876 *Two-Photon Imaging*: Two-photon imaging was performed with a resonant scanning microscope
877 (Neurolabware) using a 16x water immersion objective (Nikon CFI75 LWD 16xW 0.80NA).
878 Imaging was performed using a polymer to stabilize the immersion solution (MakingCosmetics,
879 0.4% Carbomer 940). A Ti:Sapphire laser tuned to 920nm (Spectra Physics, Mai Tai eHP
880 DeepSee) was raster scanned via a resonant galvanometer (8 kHz, Cambridge Technology) onto
881 the brain at a frame rate of either 30 Hz with a field of view of either 1030 μm x 581 μm (796 x
882 264 pixels) or 555 μm x 233 μm (796 x 264 pixels), or 15.5Hz with a field of view of 555 μm x 452
883 μm and (796 x 512 pixels). Data were collected through a green filter (510 ± 42 nm band filter
884 (Semrock)) onto GaAsP photomultipliers (H10770B-40, Hamamatsu) using Scanbox software
885 (Neurolabware). A total of 12 mice were used for imaging experiments (10 mice for wide-field, 11
886 mice for two-photon, 12 mice total).
887
888 Single Unit Recordings and Optogenetics
889 Acute single unit recordings were performed in awake animals by performing a craniotomy over
890 lobule simplex and inserting a multi-electrode silicone probe (Neuronexus, A4x8-5mm-100-400-
891 177-A32, 4 shanks, 8 site/shank at 100 μm spacing) using a Cerebus multichannel acquisition
892 system (Blackrock Microsystems, Salt Lake City). For single unit recordings obtained in the cue
893 prediction condition (Supp. Fig. 6), chronically implanted electrode arrays were used (Dual drive
894 movable electrode bundles with 8 tungsten electrodes (23 μm) in each cannula or 16 tungsten
895 electrodes bundle in one cannula, Innovative Neurophysioloy Inc). Electrode arrays were
896 implanted using stereotaxic coordinates to target lobule simplex at AP 6.2; ML 2.0. Electrode

897 bundles were inserted into lobule simplex at a depth of approximately 0.2-0.3 mm. The implant
898 was encased in Metabond for stability.
899 For both recording conditions, continuous recording data was bandpass filtered with a 2-
900 pole Butterworth between 250 Hz and 5 kHz and referenced against an electrode with no spikes
901 using Spike2. Single units were isolated by amplitude thresholding. Template waveforms were
902 defined and characterized by their width and peak, and PCA of waveforms was done in off-line in
903 Spike2.
904 Complex spikes and simple spikes were discriminated as in de Solages et al.[61], first on
905 the basis of their stereotypical waveform. Complex spikes typically had a multi-wavelet form,
906 including a large positive peak within 6ms following spike initiation. Manual identification of 10-
907 20 complex spikes was used to generate a mean template waveform, which was then compared
908 to all other spikes for a given unit using the Spearman rank order correlation coefficient. The
909 combination of Spearman coefficients and the magnitude of the positive waveform deflection was
910 used to segregate complex and simple spikes. The presence of a post-complex spike pause (20
911 ms or more) in simple spike firing was verified by cross-correlogram for all isolated single units.
912 Complex spike rates for the cue prediction condition were normalized to the baseline firing rate
913 determined in a one-second window during the ITI according to: (FR-baseline)/baseline) (Supp.
914 Fig. 6).
915 For optogenetic mapping of the dorsal cerebellum, an optical fiber (0.39 NA, 400 μm core
916 multimode, ThorLabs FT400EMT) coupled to a 532 nm laser (Optoengine, MGL-III-532) was
917 positioned above the cranial window using a micromanipulator (Scientifica PatchStar).
918
919 Histology
920 Mice were deeply anesthetized with ketamine/xylazine (200mg/kg & 30mg/kg respectively, IP)
921 then perfused with PBS then 4% paraformaldehyde. 100um sagittal sections were cut using a
922 vibratome (Pelco 102). Cerebellar slices were then mounted using a mounting medium (Southern
923 Biotech Fluoromount-G or DAPI Fluoromount-G) and imaged with a fluorescence microscope
924 (Nikon Eclipse 80i).
925
926 Data Analysis
927 *Behavior:* Behavior sessions were only analyzed within the time range of active task
928 performance. Accordingly, the last trial of each session was determined by the occurrence of
929 either two consecutive failed trials (in which the mouse did not release the lever in response to
930 the cue) or two consecutive trials with post-ITI duration to press longer than 1.5x the session
931 average.

Reaction times were measured using lever releases within the reward window as well as those occurring 200ms prior to the reward cue to account for predictive responses. Reaction times are plotted as a binned average of five trials. Initial reaction times were calculated according to the y-intercept of the linear regression of the first fifty trials. Final reaction time at the end of each session was calculated by averaging the reaction times of trials 200-250.

The symmetry of reaction time data about the sample mean was measured to test the extinguishment of learning after following cue prediction sessions according to skewness. Sample skewness was defined by

$$s = \frac{E(\mu - X)^3}{\sigma^3}$$

where μ is the mean of X, $E(*)$ is the expected value of the quantity $*$, and σ is the standard deviation of X. Thus, for a given sample x, this calculates:

$$\frac{\frac{1}{n}\sum_{i=1}^{n}(x_i - \bar{x})^3}{\left(\sqrt{\frac{1}{n}\sum_{i=1}^{n}(x_i - \bar{x})^2}\right)^3}$$

for $x_i \in x$, where $\bar{x}$ is the sample mean.

Movement trajectories were measured using a lever affixed to a rotary encoder (US Digital) with a 60mm radius and 1250 pulses per revolution. Encoder values were collected at 1000 Hz, and trajectories were calculated by up-sampling at 200 μs (5000 Hz) using nearest-neighbor interpolation. Pulse number was converted to degrees, and the vertical displacement in millimeters was calculated using the chord length of the leaver displacement angle. 20-80% rise times were calculated using normalized average trajectories. Presses and releases were sorted according to duration in a window from 200ms before threshold crossing to the time of a threshold crossing half way between the top and bottom of the total lever displacement.

Wide-field imaging: Imaging analysis were performed using custom MATLAB code. Regions of interest (ROIs) were selected within empirically defined forelimb movement region of lobule simplex according to the spread of GCaMP expression. Window location and the lobule identity were identified according to folia patterns visible through the cranial window, landmarks recorded during surgery, and post-hoc histology. Baseline fluorescence (F) was measured on a trial-by-trial basis during the inter-trial interval (ITI) as the mean fluorescence 900 to 200ms before trial initiation. Normalized fluorescence (ΔF/F) was calculated according to the cumulative activity within an ROI, or on a pixel by pixel basis. Lever hold times <200ms in total, or > 1 s after the

visual cue were exceedingly rare, and thus excluded from analysis. Lever releases between 200ms and 1000ms following the visual cue were classified as correct, and releases prior to visual cue were classified as early. Lever releases ≤200 ms following the visual cue were considered too fast to be reactions to the cue based on average reaction time distributions. Peak ΔF/F was measured on a trial by trial basis in the time window from 100ms before to 400 ms after lever release. Note that differences in the timing of single trial calcium transient peaks produce smaller amplitudes for ΔF/F timecourses as compared to reported peak ΔF/F measurements. Spearman's correlation between lick rate and peak ΔF/F within sessions was calculated according to the lick rate within 500 ms following each lever release and the peak calcium transient for each trial. For this correlation analysis, trials without licking were removed, and only sessions with 7 or more trials in each condition were included.

Meta K-means analysis and Cluster Correlations: Images were first registered to reduce motion artifacts, and then thresholded at 70% of maximum intensity for each frame to remove background noise. Images were downsampled 5-fold in both X and Y. Baseline F was defined as the averaged fluorescence across the entire movie for each pixel, and used to normalize change in fluorescence (ΔF/F). ΔF/F was then re-normalized to the maximum ΔF/F during the entire movie for each pixel. The repeated k-means clustering algorithm (meta-k-means) separated pixels to cluster centroids based on a pairwise correlation distance function using Pearson's linear correlation coefficient (r). The final clusters were determined by first thresholding all the k-means results at 800 out of 1000 runs, and then by merging highly correlated clusters based on Dunn's index. Clusters occupying less than 3% of the total imaging field were excluded from further analysis. Intra-cluster and inter-cluster correlation coefficients were calculated between 100 ms before and 300 ms after lever release for both correct and early trials on a frame by frame basis. To test for differences in the relationship between spike rates and correlation coefficients between trial types, paired clusters from each distribution were resampled with replacement and fit with a line to measure the y-intercept 1000 times. Statistical significance was computed according to the 95% confidence interval of the distribution of y-intercept difference values (difference between y-intercepts 0.0375 ± 0.0013, 95% confidence interval [0.0349, 0.0402]).

Two-photon imaging: Motion in the XY plane was corrected by sub-pixel image registration. To isolate signals from individual PC dendrites, we utilized principal component analysis (PCA) followed by independent component analysis (ICA). Final dendrite segmentation was achieved by thresholding the smoothed spatial filters from ICA. A binary mask was created by combining highly correlated pixels (correlation coefficient > 0.8) and removing any overlapped regions between segmented dendrites. Notably, image segmentation using these criteria did not extract

1001 PC soma, which were clearly visible in many single- and two-photon imaging experiments.
1002 Fluorescence changes (ΔF) were normalized to a window of baseline fluorescence (F) between
1003 500ms and 100ms preceding trial initiation. Responses were categorized as significant ($p<0.05$)
1004 according to a one-tailed t-test if the $\Delta F/F$ in a 200 ms window surrounding lever press or release
1005 was larger than that from a 500 ms window immediately preceding lever movement. To extract
1006 events on single trials used for estimation of complex spike rates and event amplitudes, the first
1007 derivative of the raw fluorescence trace was thresholded at 2.5 standard deviations from baseline.
1008 The same methods were used to extract events for the subset of single photon experiments
1009 described in Supp. Fig. 5. For single trial amplitude measurements, only events well separated
1010 in time (greater than 650ms from the next event) were considered; however, for measurements
1011 of rates, all events separated by at least one frame were included. Note that rate estimates are
1012 thus likely to be lower than actual rates, particularly for single photon imaging where data were
1013 collected at 100 ms intervals. For measurements of standard deviation of event times, events
1014 were extracted from a window 433 ms around the lever release, and independently aligned to the
1015 time of visual cue. The same criteria were applied to electrophysiological measurements of spike
1016 times. Event latencies were calculated according to the time of peak event probability. Peak
1017 calcium transients on reward omission trials and on early release trials were quantified in two time
1018 windows (Fig. 8). Window 1 spanned the first 100 ms after lever release, and window 2 spanned
1019 175 ms that began 165ms after lever release. Spearman's correlation was calculated between
1020 lick rate and the peak calcium transient within sessions on a frame by frame basis for each trial
1021 in a window spanning 500 ms after lever release. Correlation values for correct and early release
1022 trials for each cell were averaged separately. Some neurons showed responses to licking, as
1023 defined by a mean lick-triggered calcium transient (for cells with at least 4 lick events per session)
1024 that was significantly larger ($p<0.05$) with respect to baseline (Supp. Fig. 7). Lick triggered
1025 averages were constructed from licks presumed to be spontaneous that occurred during the inter-
1026 trial interval with a buffer of 1000 ms between the end of the previous trial and the start of analysis
1027 to avoid contamination of reward-related licking.
1028
1029 *Additional statistics and data sharing*: Data are presented as mean ± S.E.M., unless stated
1030 otherwise. Statistical tests were two-sided, and analyses of variance (ANOVA) were performed
1031 when more than two groups were tested. Differences were considered statistically significant
1032 when $P < 0.05$. No correction for multiple comparisons was applied. No statistical methods were
1033 used to predetermine sample sizes. Data collection and analysis were not performed blind to the
1034 conditions of the experiments, but data collection relied on automatized measurements and
1035 subsequent analysis was based on code uniformly applied across experimental conditions. Data

analysis code are available on GitHub (access available upon request). The data that support the findings of this study are available from the corresponding author upon reasonable request.

References

1. Albus, J.S. A theory of cerebellar function. *Mathematical Biosciences* **10**, 25-61 (1971).
2. Ito, M. Neural design of the cerebellar motor control system. *Brain Res* **40**, 81-84 (1972).
3. Marr, D. A theory of cerebellar cortex. *J Physiol* **202**, 437-470 (1969).
4. Ito, M., Sakurai, M. & Tongroach, P. Climbing fibre induced depression of both mossy fibre responsiveness and glutamate sensitivity of cerebellar Purkinje cells. *J Physiol* **324**, 113-134 (1982).
5. Ekerot, C.F. & Kano, M. Long-term depression of parallel fibre synapses following stimulation of climbing fibres. *Brain Res* **342**, 357-360 (1985).
6. Sakurai, M. Synaptic modification of parallel fibre-Purkinje cell transmission in in vitro guinea-pig cerebellar slices. *J Physiol* **394**, 463-480 (1987).
7. Miyakawa, H., Lev-Ram, V., Lasser-Ross, N. & Ross, W.N. Calcium transients evoked by climbing fiber and parallel fiber synaptic inputs in guinea pig cerebellar Purkinje neurons. *J Neurophysiol* **68**, 1178-1189 (1992).
8. Tank, D.W., Sugimori, M., Connor, J.A. & Llinas, R.R. Spatially resolved calcium dynamics of mammalian Purkinje cells in cerebellar slice. *Science* **242**, 773-777 (1988).
9. Konnerth, A., Dreessen, J. & Augustine, G.J. Brief dendritic calcium signals initiate long-lasting synaptic depression in cerebellar Purkinje cells. *Proc Natl Acad Sci U S A* **89**, 7051-7055 (1992).
10. Llinas, R. & Sugimori, M. electrophysiological properties of in vitro purkinje cell somata in mammalian cerebellar slices. *J. Physiol.*, 171-195 (1980).
11. Eccles, J.C., Llinas, R. & Sasaki, K. The excitatory synaptic action of climbing fibres on the Purkinje cells of the cerebellum. *J Physiol* **182**, 268-296 (1966).
12. Medina, J.F., Nores, W.L., Ohyama, T. & Mauk, M.D. Mechanisms of cerebellar learning suggested by eyelid conditioning. *Current opinion in neurobiology* **10**, 717-724 (2000).
13. Ohyama, T.N.W.M.M. & Mauk, M. What the cerebellum computes. *Trends in Neurosciences* **26**, 222-227 (2003).

1068 14. Raymond, J.L., Lisberger, S.G. & Mauk, M.D. The cerebellum: a neuronal learning
1069 machine? *Science* **272**, 1126-1131 (1996).
1070 15. Schultz, S.R., Kitamura, K., Post-Uiterweer, A., Krupic, J. & Hausser, M. Spatial pattern
1071 coding of sensory information by climbing fiber-evoked calcium signals in networks of
1072 neighboring cerebellar Purkinje cells. *J Neurosci* **29**, 8005-8015 (2009).
1073 16. Tsutsumi, S*., et al.* Structure-function relationships between aldolase C/zebrin II
1074 expression and complex spike synchrony in the cerebellum. *J Neurosci* **35**, 843-852 (2015).
1075 17. Ozden, I., Dombeck, D.A., Hoogland, T.M., Tank, D.W. & Wang, S.S. Widespread state-
1076 dependent shifts in cerebellar activity in locomoting mice. *PLoS One* **7**, e42650 (2012).
1077 18. De Gruijl, J.R., Hoogland, T.M. & De Zeeuw, C.I. Behavioral correlates of complex spike
1078 synchrony in cerebellar microzones. *J Neurosci* **34**, 8937-8947 (2014).
1079 19. Tang, T., Suh, C.Y., Blenkinsop, T.A. & Lang, E.J. Synchrony is Key: Complex Spike Inhibition
1080 of the Deep Cerebellar Nuclei. *Cerebellum* **15**, 10-13 (2016).
1081 20. Lee, K.H*., et al.* Circuit mechanisms underlying motor memory formation in the
1082 cerebellum. *Neuron* **86**, 529-540 (2015).
1083 21. Histed, M.H., Carvalho, L.A. & Maunsell, J.H. Psychophysical measurement of contrast
1084 sensitivity in the behaving mouse. *J Neurophysiol* **107**, 758-765 (2012).
1085 22. Chettih, S.N., McDougle, S.D., Ruffolo, L.I. & Medina, J.F. Adaptive timing of motor output
1086 in the mouse: the role of movement oscillations in eyelid conditioning. *Front Integr Neurosci* **5**,
1087 72 (2011).
1088 23. Gaffield, M.A., Amat, S.B., Bito, H. & Christie, J.M. Chronic imaging of movement-related
1089 Purkinje cell calcium activity in awake behaving mice. *J Neurophysiol* **115**, 413-422 (2016).
1090 24. Mukamel, E.A., Nimmerjahn, A. & Schnitzer, M.J. Automated analysis of cellular signals
1091 from large-scale calcium imaging data. *Neuron* **63**, 747-760 (2009).
1092 25. Najafi, F., Giovannucci, A., Wang, S.S. & Medina, J.F. Coding of stimulus strength via analog
1093 calcium signals in Purkinje cell dendrites of awake mice. *Elife* **3**, e03663 (2014).
1094 26. Ozden, I., Lee, H.M., Sullivan, M.R. & Wang, S.S. Identification and clustering of event
1095 patterns from in vivo multiphoton optical recordings of neuronal ensembles. *J Neurophysiol* **100**,
1096 495-503 (2008).

1097 27. Ozden, I., Sullivan, M.R., Lee, H.M. & Wang, S.S. Reliable coding emerges from
1098 coactivation of climbing fibers in microbands of cerebellar Purkinje neurons. *J Neurosci* **29**,
1099 10463-10473 (2009).
1100 28. Najafi, F., Giovannucci, A., Wang, S.S. & Medina, J.F. Sensory-driven enhancement of
1101 calcium signals in individual Purkinje cell dendrites of awake mice. *Cell Rep* **6**, 792-798 (2014).
1102 29. Najafi, F. & Medina, J.F. Beyond "all-or-nothing" climbing fibers: graded representation of
1103 teaching signals in Purkinje cells. *Front Neural Circuits* **7**, 115 (2013).
1104 30. Yang, Y. & Lisberger, S.G. Purkinje-cell plasticity and cerebellar motor learning are graded
1105 by complex-spike duration. *Nature* **510**, 529-532 (2014).
1106 31. Rudolph, S., Overstreet-Wadiche, L. & Wadiche, J.I. Desynchronization of multivesicular
1107 release enhances Purkinje cell output. *Neuron* **70**, 991-1004 (2011).
1108 32. Maruta, J., Hensbroek, R.A. & Simpson, J.I. Intraburst and interburst signaling by climbing
1109 fibers. *J Neurosci* **27**, 11263-11270 (2007).
1110 33. Kitamura, K. & Hausser, M. Dendritic calcium signaling triggered by spontaneous and
1111 sensory-evoked climbing fiber input to cerebellar Purkinje cells in vivo. *J Neurosci* **31**, 10847-
1112 10858 (2011).
1113 34. Brenowitz, S.D. & Regehr, W.G. Associative short-term synaptic plasticity mediated by
1114 endocannabinoids. *Neuron* **45**, 419-431 (2005).
1115 35. Eilers, J., Augustine, G.J. & Konnerth, A. Subthreshold synaptic Ca2+ signalling in fine
1116 dendrites and spines of cerebellar Purkinje neurons. *Nature* **373**, 155-158 (1995).
1117 36. Hartell, N.A. Strong activation of parallel fibers produces localized calcium transients and
1118 a form of LTD that spreads to distant synapses. *Neuron* **16**, 601-610 (1996).
1119 37. Wang, S.S., Denk, W. & Hausser, M. Coincidence detection in single dendritic spines
1120 mediated by calcium release. *Nat Neurosci* **3**, 1266-1273 (2000).
1121 38. Andersson, G. & Oscarsson, O. Climbing fiber microzones in cerebellar vermis and their
1122 projection to different groups of cells in the lateral vestibular nucleus. *Exp Brain Res* **32**, 565-579
1123 (1978).
1124 39. Apps, R. & Garwicz, M. Anatomical and physiological foundations of cerebellar
1125 information processing. *Nat Rev Neurosci* **6**, 297-311 (2005).
1126 40. Ohmae, S. & Medina, J.F. Climbing fibers encode a temporal-difference prediction error
1127 during cerebellar learning in mice. *Nat Neurosci* **18**, 1798-1803 (2015).

1128 41. Ackerley, R., Pardoe, J. & Apps, R. A novel site of synaptic relay for climbing fibre pathways
1129 relaying signals from the motor cortex to the cerebellar cortical C1 zone. *J Physiol* **576**, 503-518
1130 (2006).
1131 42. Kitazawa, S., Kimura, T. & Yin, P.B. Cerebellar complex spikes encode both destinations
1132 and errors in arm movements. *Nature* **392**, 494-497 (1998).
1133 43. Sugihara, I. & Shinoda, Y. Molecular, topographic, and functional organization of the
1134 cerebellar cortex: a study with combined aldolase C and olivocerebellar labeling. *J Neurosci* **24**,
1135 8771-8785 (2004).
1136 44. Sugihara, I., Wu, H.S. & Shinoda, Y. The entire trajectories of single olivocerebellar axons
1137 in the cerebellar cortex and their contribution to Cerebellar compartmentalization. *J Neurosci* **21**,
1138 7715-7723 (2001).
1139 45. Voogd, J., Pardoe, J., Ruigrok, T.J. & Apps, R. The distribution of climbing and mossy fiber
1140 collateral branches from the copula pyramidis and the paramedian lobule: congruence of
1141 climbing fiber cortical zones and the pattern of zebrin banding within the rat cerebellum. *J*
1142 *Neurosci* **23**, 4645-4656 (2003).
1143 46. Ekerot, C.F., Garwicz, M. & Schouenborg, J. Topography and nociceptive receptive fields
1144 of climbing fibres projecting to the cerebellar anterior lobe in the cat. *J Physiol* **441**, 257-274
1145 (1991).
1146 47. Oberdick, J., Baader, S.L. & Schilling, K. From zebra stripes to postal zones: deciphering
1147 patterns of gene expression in the cerebellum. *Trends Neurosci* **21**, 383-390 (1998).
1148 48. Zhou, H.*, et al.* Cerebellar modules operate at different frequencies. *Elife* **3**, e02536
1149 (2014).
1150 49. Paukert, M., Huang, Y.H., Tanaka, K., Rothstein, J.D. & Bergles, D.E. Zones of enhanced
1151 glutamate release from climbing fibers in the mammalian cerebellum. *J Neurosci* **30**, 7290-7299
1152 (2010).
1153 50. Blenkinsop, T.A. & Lang, E.J. Synaptic action of the olivocerebellar system on cerebellar
1154 nuclear spike activity. *J Neurosci* **31**, 14708-14720 (2011).
1155 51. Bengtsson, F., Ekerot, C.F. & Jorntell, H. In vivo analysis of inhibitory synaptic inputs and
1156 rebounds in deep cerebellar nuclear neurons. *PLoS One* **6**, e18822 (2011).
1157 52. Person, A.L. & Raman, I.M. Purkinje neuron synchrony elicits time-locked spiking in the
1158 cerebellar nuclei. *Nature* **481**, 502-505 (2012).

1159 53. McElvain, L.E., Bagnall, M.W., Sakatos, A. & du Lac, S. Bidirectional plasticity gated by
1160 hyperpolarization controls the gain of postsynaptic firing responses at central vestibular nerve
1161 synapses. *Neuron* **68**, 763-775 (2010).
1162 54. Pugh, J.R. & Raman, I.M. Potentiation of mossy fiber EPSCs in the cerebellar nuclei by
1163 NMDA receptor activation followed by postinhibitory rebound current. *Neuron* **51**, 113-123
1164 (2006).
1165 55. Miles, F.A. & Lisberger, S.G. Plasticity in the vestibulo-ocular reflex: a new hypothesis.
1166 *Annu Rev Neurosci* **4**, 273-299 (1981).
1167 56. Matias, S., Lottem, E., Dugue, G.P. & Mainen, Z.F. Activity patterns of serotonin neurons
1168 underlying cognitive flexibility. *Elife* **6** (2017).
1169 57. Belova, M.A., Paton, J.J., Morrison, S.E. & Salzman, C.D. Expectation modulates neural
1170 responses to pleasant and aversive stimuli in primate amygdala. *Neuron* **55**, 970-984 (2007).
1171 58. Hayden, B.Y., Heilbronner, S.R., Pearson, J.M. & Platt, M.L. Surprise signals in anterior
1172 cingulate cortex: neuronal encoding of unsigned reward prediction errors driving adjustment in
1173 behavior. *J Neurosci* **31**, 4178-4187 (2011).
1174 59. Pearce, J.M. & Hall, G. A model for Pavlovian learning: variations in the effectiveness of
1175 conditioned but not of unconditioned stimuli. *Psychol Rev* **87**, 532-552 (1980).
1176 60. Roesch, M.R., Esber, G.R., Li, J., Daw, N.D. & Schoenbaum, G. Surprise! Neural correlates
1177 of Pearce-Hall and Rescorla-Wagner coexist within the brain. *Eur J Neurosci* **35**, 1190-1200 (2012).
1178 61. de Solages, C.*, et al.* High-frequency organization and synchrony of activity in the purkinje
1179 cell layer of the cerebellum. *Neuron* **58**, 775-788 (2008).
1180

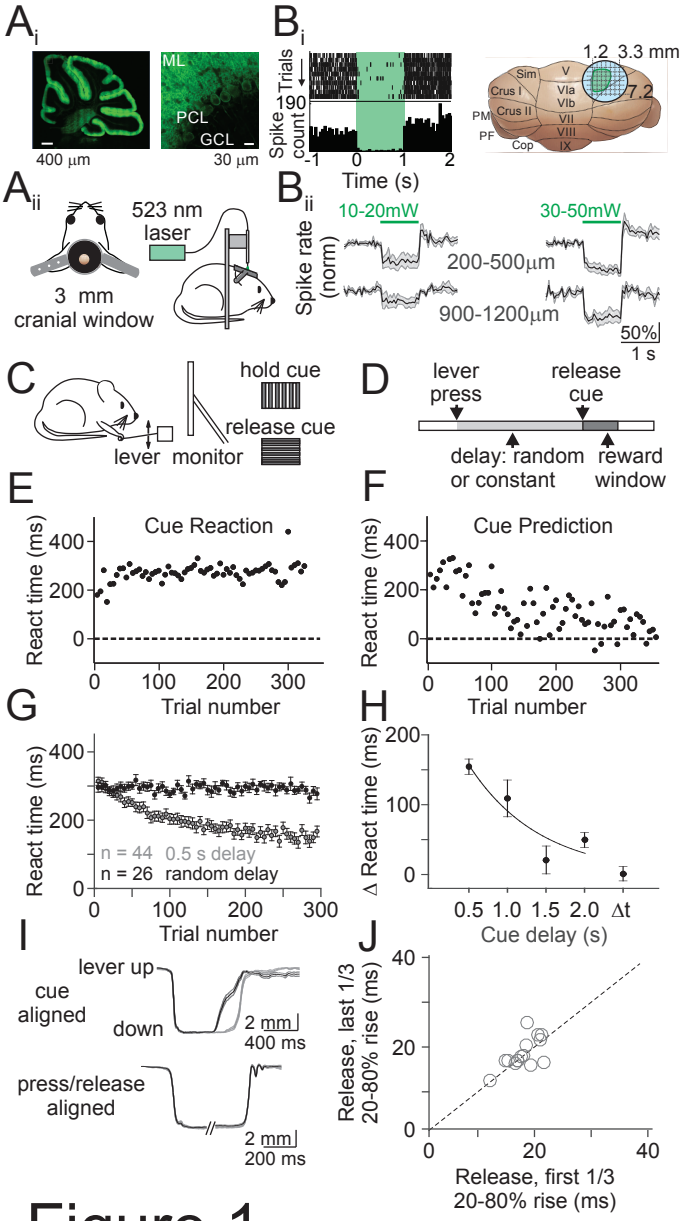
A_i
ML
PCL
GCL
400 µm
30 µm
B_i
Trials
190
Spike count
-1
0
1
2
Time (s)
1.2
3.3 mm
7.2
Sim
V
Crus I
VIa
VIb
Crus II
PM
VII
PF
VIII
Cop
IX
A_ii
523 nm laser
3 mm cranial window
B_ii
10-20mW
30-50mW
Spike rate (norm)
200-500µm
900-1200µm
50%
1 s
C
hold cue
release cue
lever
monitor
D
lever press
release cue
delay: random or constant
reward window
E
Cue Reaction
React time (ms)
400
200
0
0
100
200
300
Trial number
F
Cue Prediction
React time (ms)
400
200
0
0
100
200
300
Trial number
G
React time (ms)
400
200
0
n = 44 0.5 s delay
n = 26 random delay
0
100
200
300
Trial number
H
Δ React time (ms)
200
100
0
0.5
1.0
1.5
2.0
Δt
Cue delay (s)
I
lever up
cue aligned
down
2 mm
400 ms
press/release aligned
2 mm
200 ms
J
Release, last 1/3 20-80% rise (ms)
40
20
0
0
20
40
Release, first 1/3 20-80% rise (ms)

Figure 1

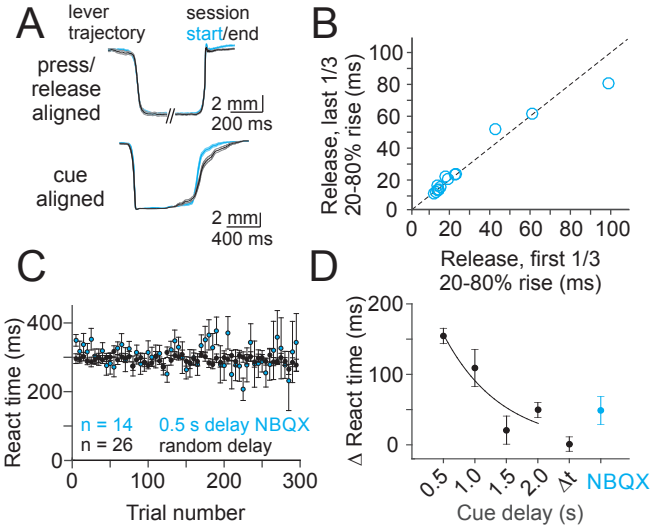
A
lever trajectory
session start/end
press/ release aligned
2 mm
200 ms
cue aligned
2 mm
400 ms
B
Release, last 1/3 20-80% rise (ms)
Release, first 1/3 20-80% rise (ms)
C
React time (ms)
n = 14
n = 26
0.5 s delay NBQX
random delay
Trial number
D
Δ React time (ms)
0.5
1.0
1.5
2.0
Δt
NBQX
Cue delay (s)

Figure 2

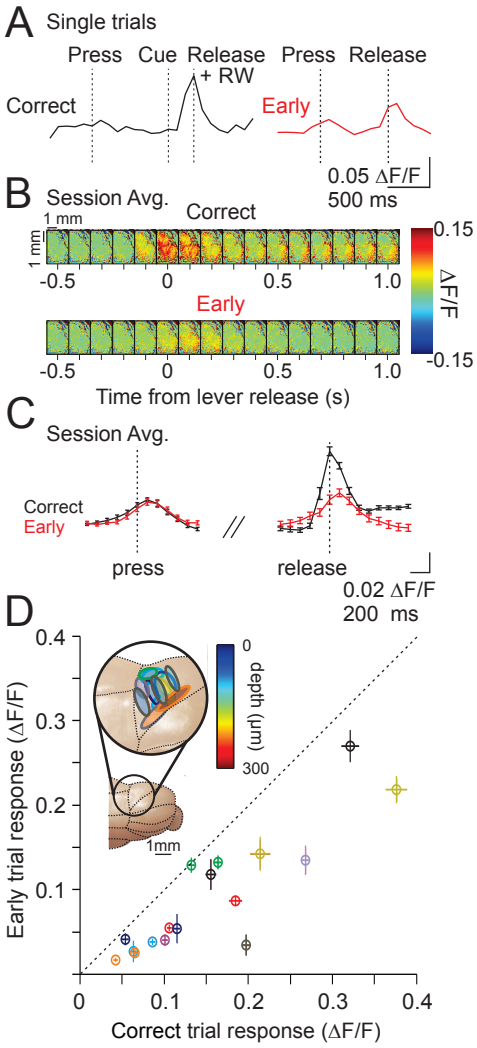
A
Single trials
Press
Cue
Release
+ RW
Press
Release
Correct
Early
0.05 ΔF/F
500 ms
B
Session Avg.
Correct
1 mm
1 mm
-0.5
0
0.5
1.0
Early
-0.5
0
0.5
1.0
0.15
ΔF/F
-0.15
Time from lever release (s)
C
Session Avg.
Correct
Early
press
release
0.02 ΔF/F
200 ms
D
0.4
0.3
0.2
0.1
Early trial response (ΔF/F)
0
0.1
0.2
0.3
0.4
Correct trial response (ΔF/F)
0
depth (μm)
300
1mm

Figure 3

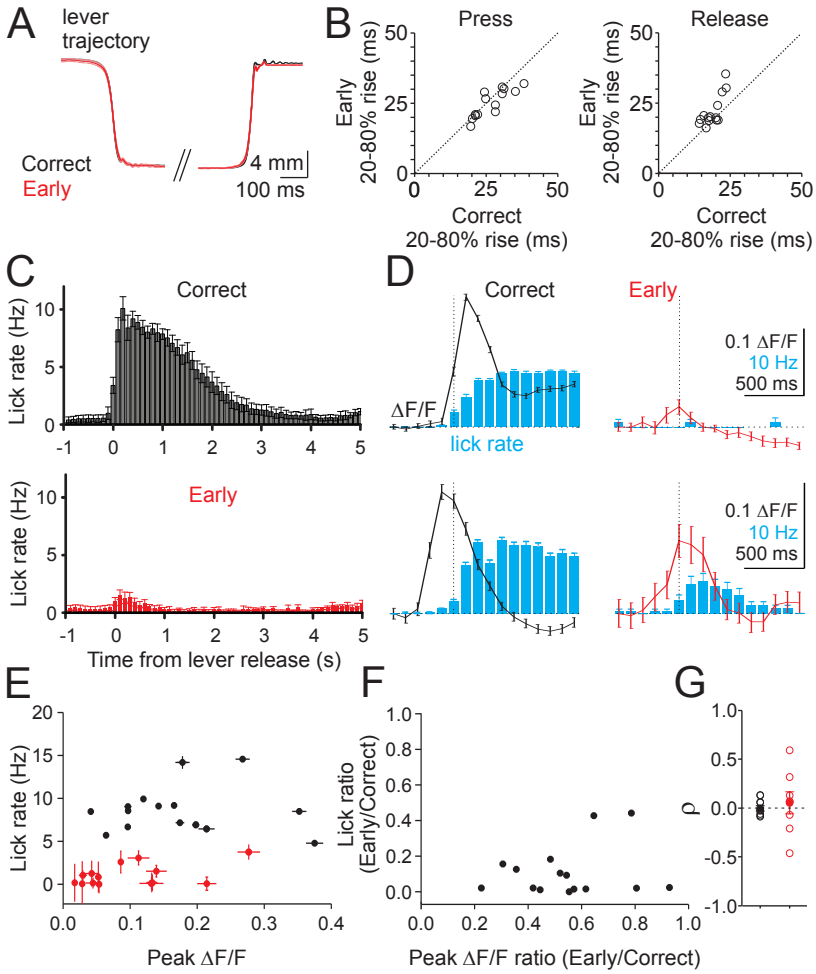
A
lever
trajectory
Correct
Early
4 mm
100 ms
B
Press
Release
Early
20-80% rise (ms)
Correct
20-80% rise (ms)
C
Correct
Early
Lick rate (Hz)
Time from lever release (s)
D
Correct
Early
ΔF/F
lick rate
0.1 ΔF/F
10 Hz
500 ms
E
Lick rate (Hz)
Peak ΔF/F
F
Lick ratio
(Early/Correct)
Peak ΔF/F ratio (Early/Correct)
G
ρ

Figure 4

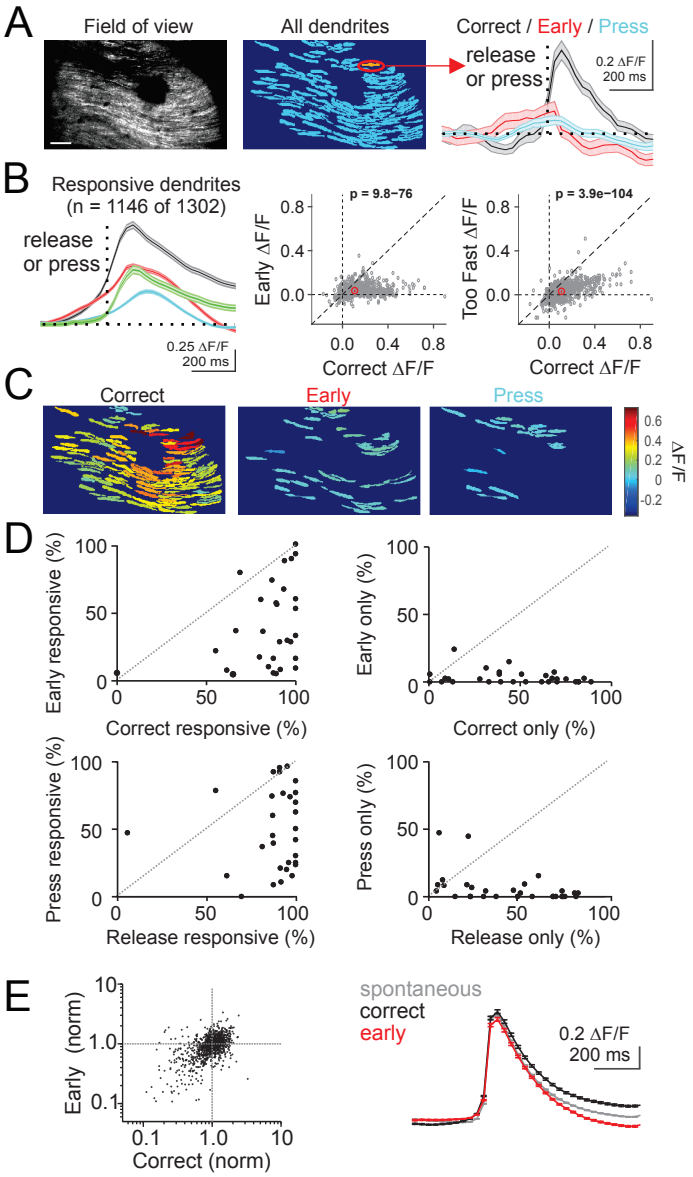
A
Field of view
All dendrites
Correct / Early / Press
release
or press
0.2 ΔF/F
200 ms
B
Responsive dendrites
(n = 1146 of 1302)
release
or press
0.25 ΔF/F
200 ms
p = 9.8−76
Early ΔF/F
Correct ΔF/F
p = 3.9e−104
Too Fast ΔF/F
Correct ΔF/F
C
Correct
Early
Press
ΔF/F
D
Early responsive (%)
Correct responsive (%)
Early only (%)
Correct only (%)
Press responsive (%)
Release responsive (%)
Press only (%)
Release only (%)
E
Early (norm)
Correct (norm)
spontaneous
correct
early
0.2 ΔF/F
200 ms

Figure 5

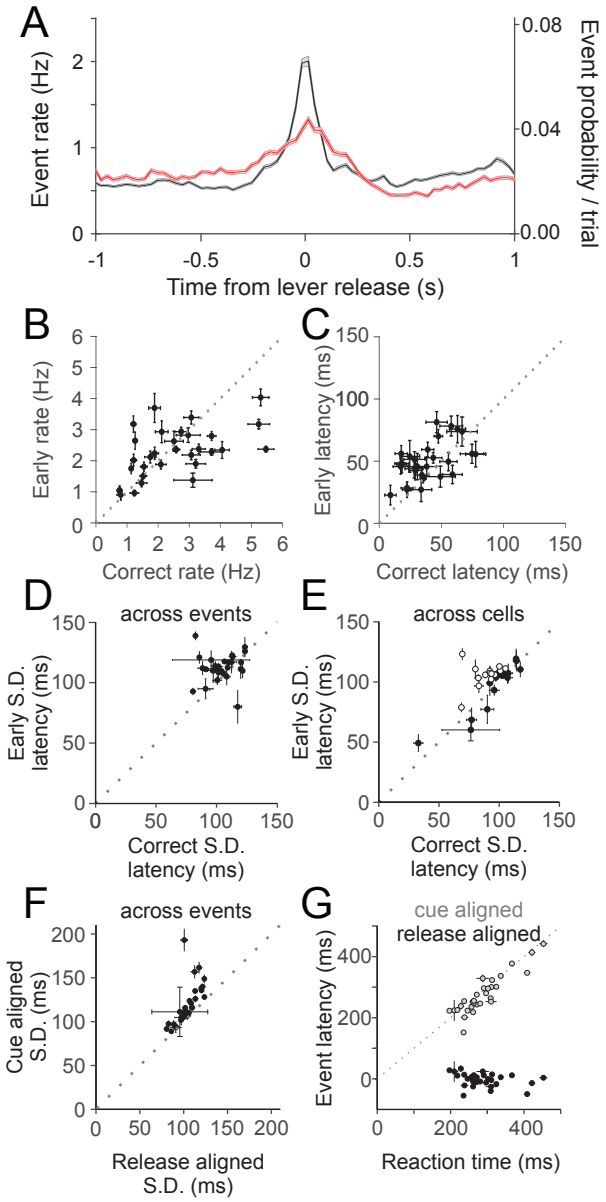
A
Event rate (Hz)
Event probability / trial
Time from lever release (s)
B
Early rate (Hz)
Correct rate (Hz)
C
Early latency (ms)
Correct latency (ms)
D
across events
Early S.D. latency (ms)
Correct S.D. latency (ms)
E
across cells
Early S.D. latency (ms)
Correct S.D. latency (ms)
F
across events
Cue aligned S.D. (ms)
Release aligned S.D. (ms)
G
cue aligned
release aligned
Event latency (ms)
Reaction time (ms)

Figure 6

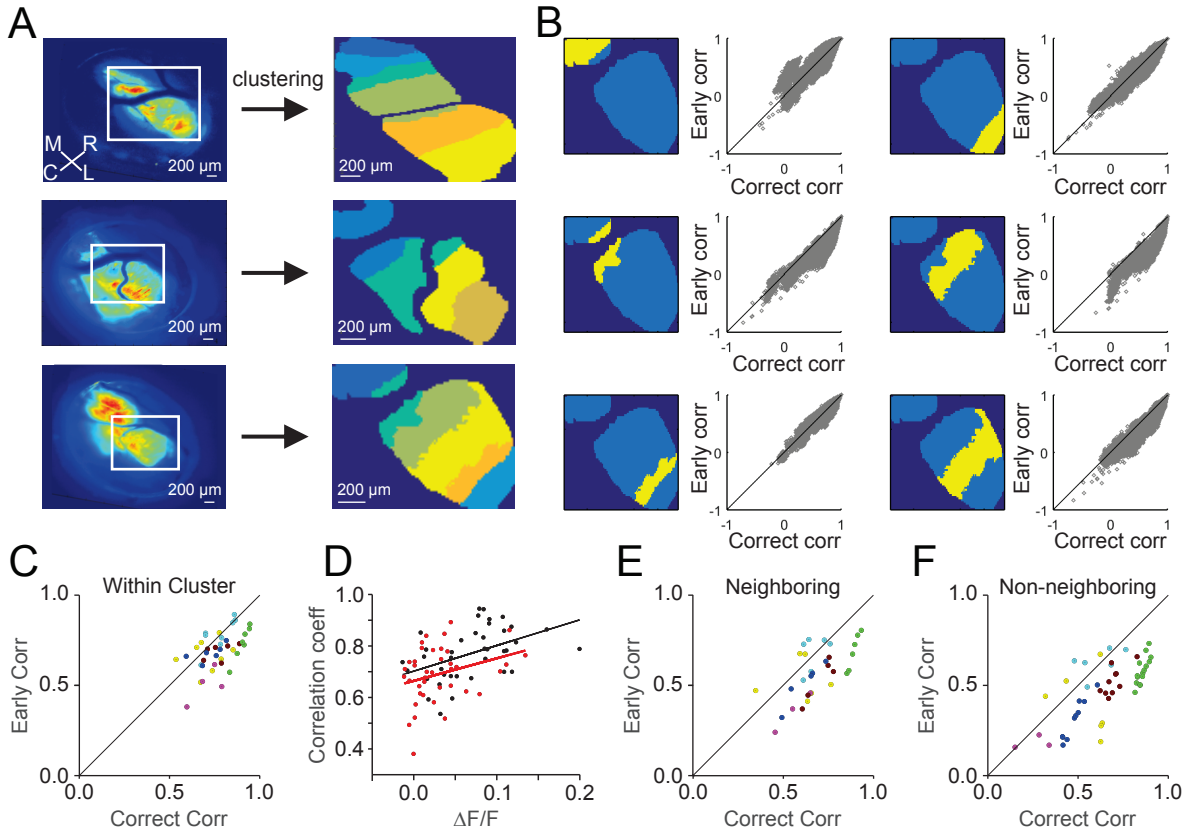
A
clustering
M
R
C
L
200 µm
B
Early corr
Correct corr
C
Within Cluster
Early Corr
Correct Corr
D
Correlation coeff
ΔF/F
E
Neighboring
F
Non-neighboring

Figure 7

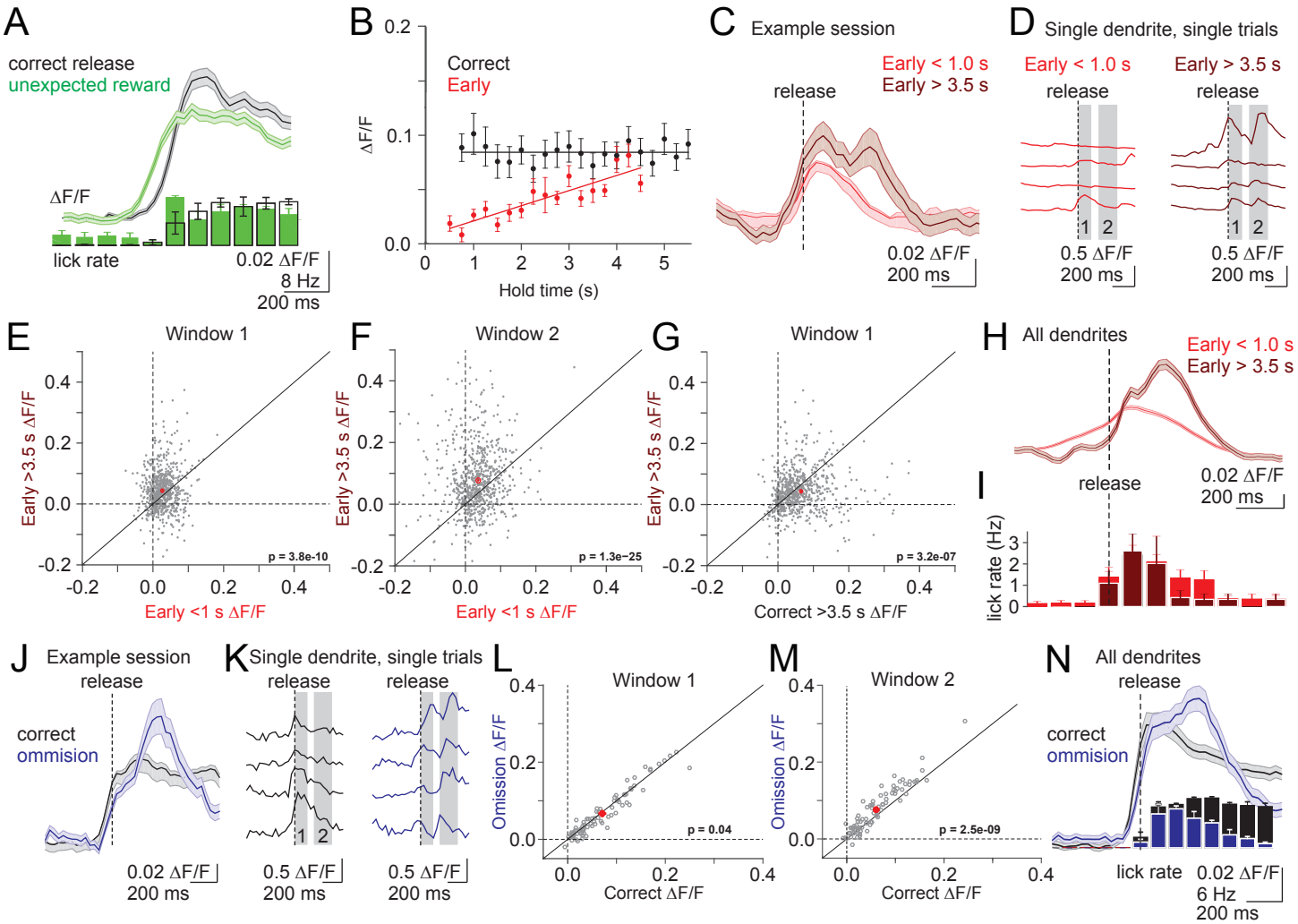
A
correct release
unexpected reward
ΔF/F
lick rate
0.02 ΔF/F
8 Hz
200 ms
B
Correct
Early
ΔF/F
Hold time (s)
C
Example session
release
Early < 1.0 s
Early > 3.5 s
0.02 ΔF/F
200 ms
D
Single dendrite, single trials
Early < 1.0 s
Early > 3.5 s
release
1
2
0.5 ΔF/F
200 ms
E
Window 1
Early >3.5 s ΔF/F
Early <1 s ΔF/F
p = 3.8e-10
F
Window 2
p = 1.3e−25
G
Window 1
Correct >3.5 s ΔF/F
p = 3.2e-07
H
All dendrites
Early < 1.0 s
Early > 3.5 s
release
0.02 ΔF/F
200 ms
I
lick rate (Hz)
J
Example session
release
correct
ommision
0.02 ΔF/F
200 ms
K
Single dendrite, single trials
release
0.5 ΔF/F
200 ms
L
Window 1
Omission ΔF/F
Correct ΔF/F
p = 0.04
M
Window 2
p = 2.5e-09
N
All dendrites
release
correct
ommision
lick rate
0.02 ΔF/F
6 Hz
200 ms

Figure 8

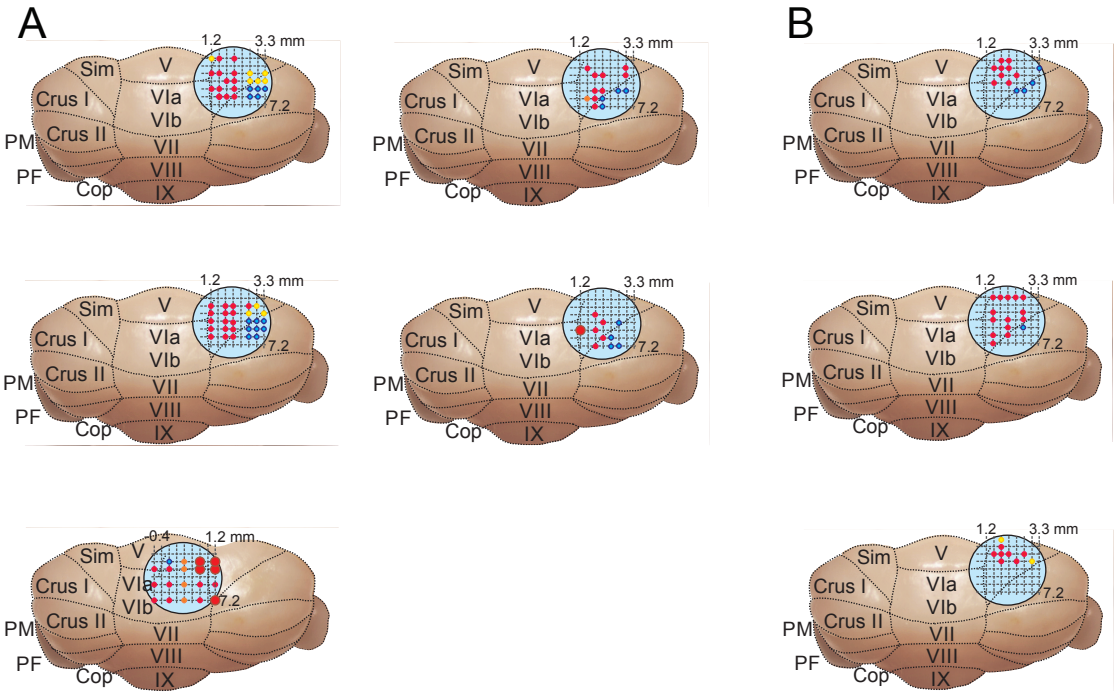

Arch: 5 mice
10-50mW, one Step pulse for 1sec

Right arm
Right & Left arms
Very weak arm movements
Whiskers or mouth or nose
nothing

Electrical Stim. 3 mice
0.1mA-1mA
50Hz for 500ms or 1sec

Right arm
Right & Left arms
Very weak arm movements
Whiskers or mouth or nose
nothing

supplemental figure 1

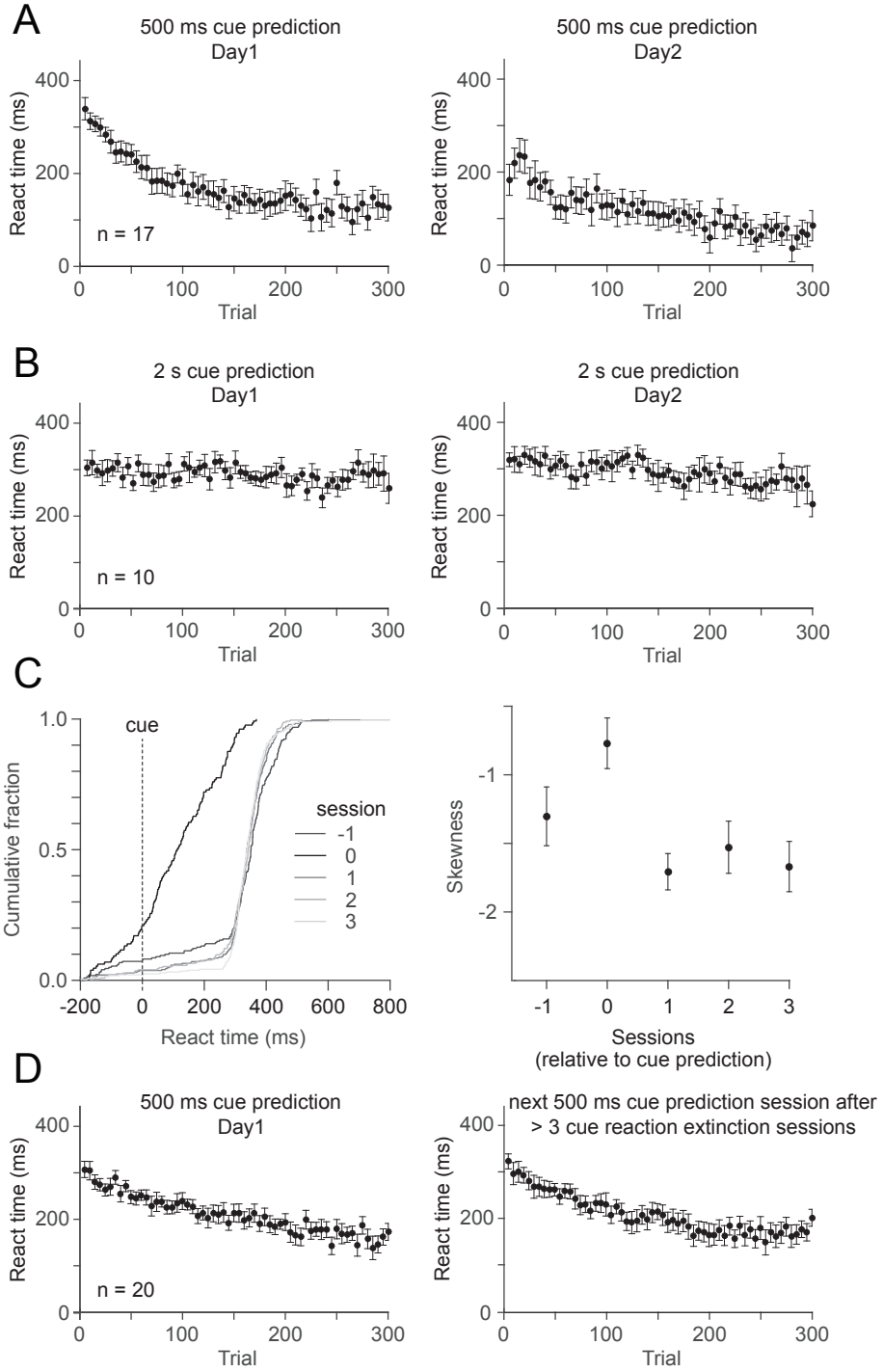

supplemental figure 2

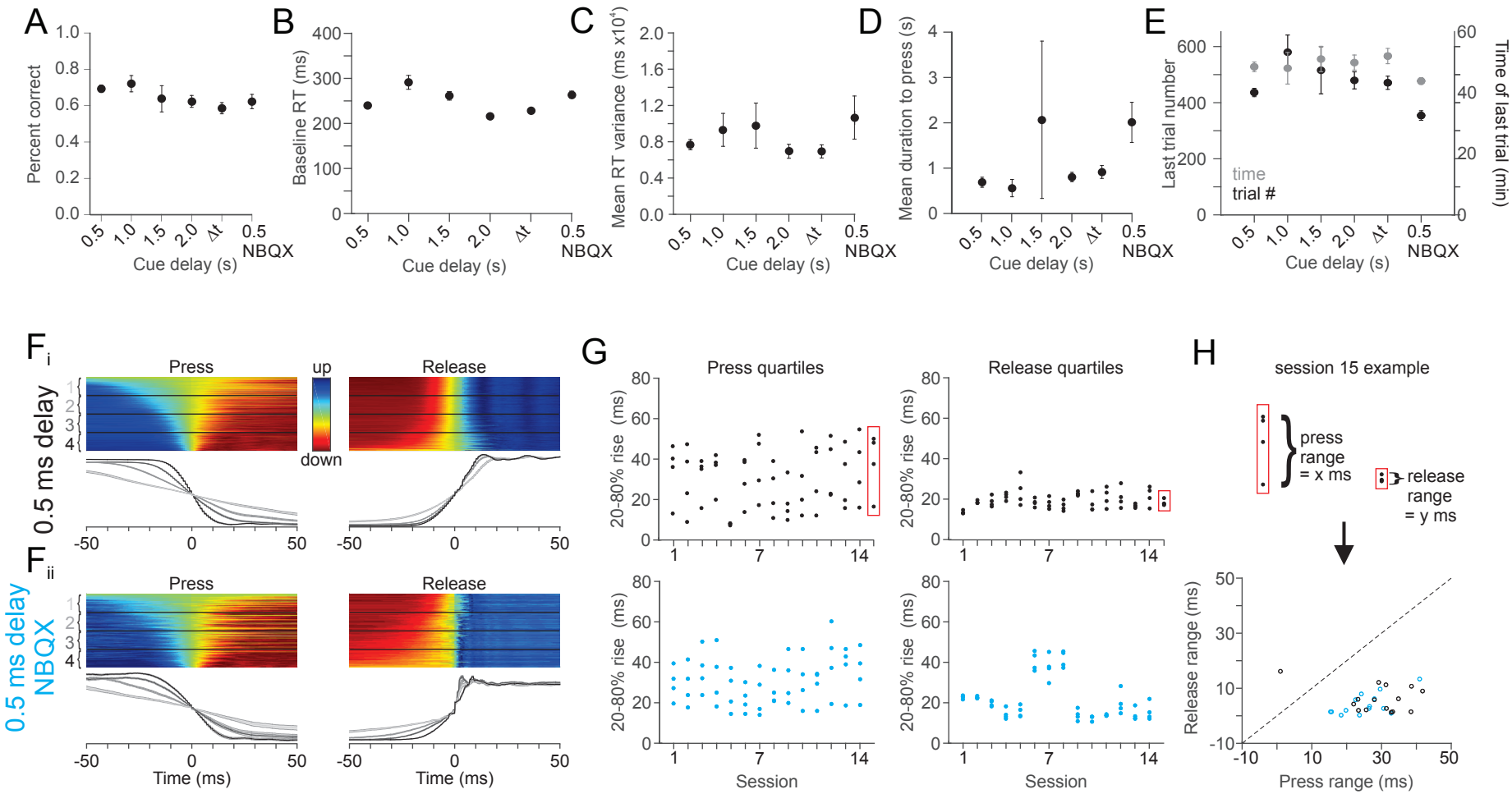

supplemental figure 3

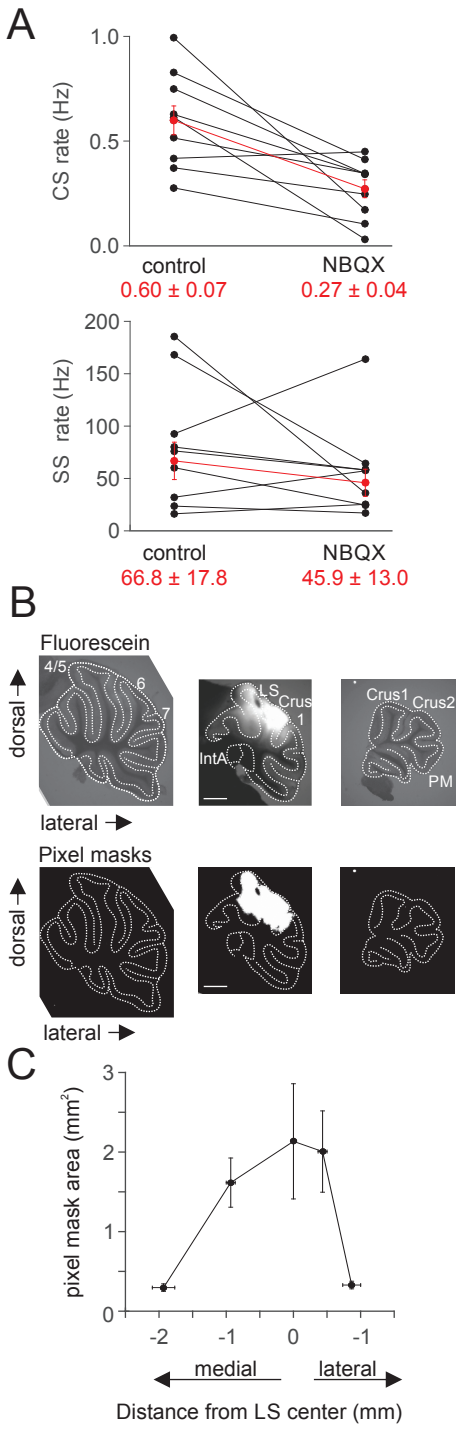

supplemental figure 4

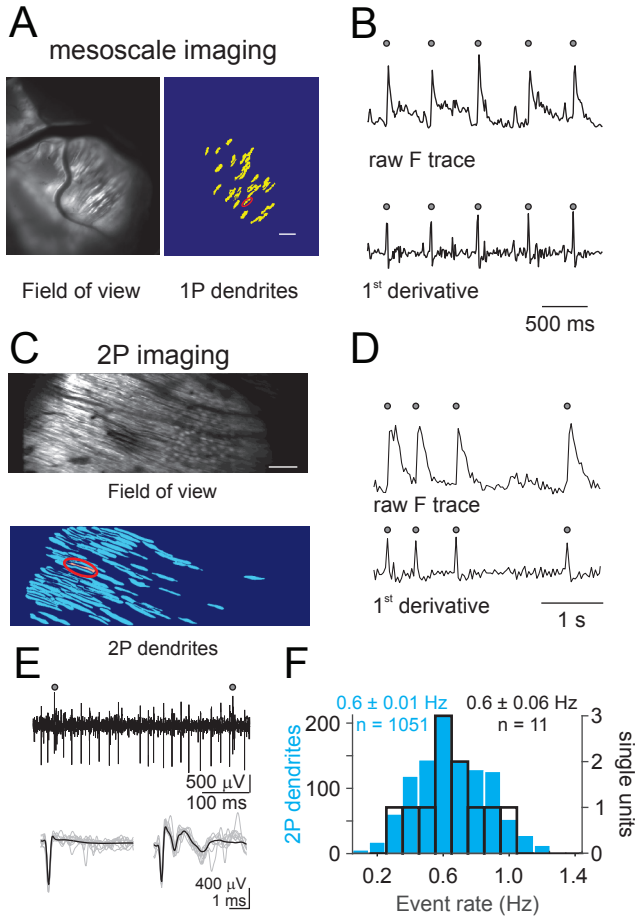

supplemental figure 5

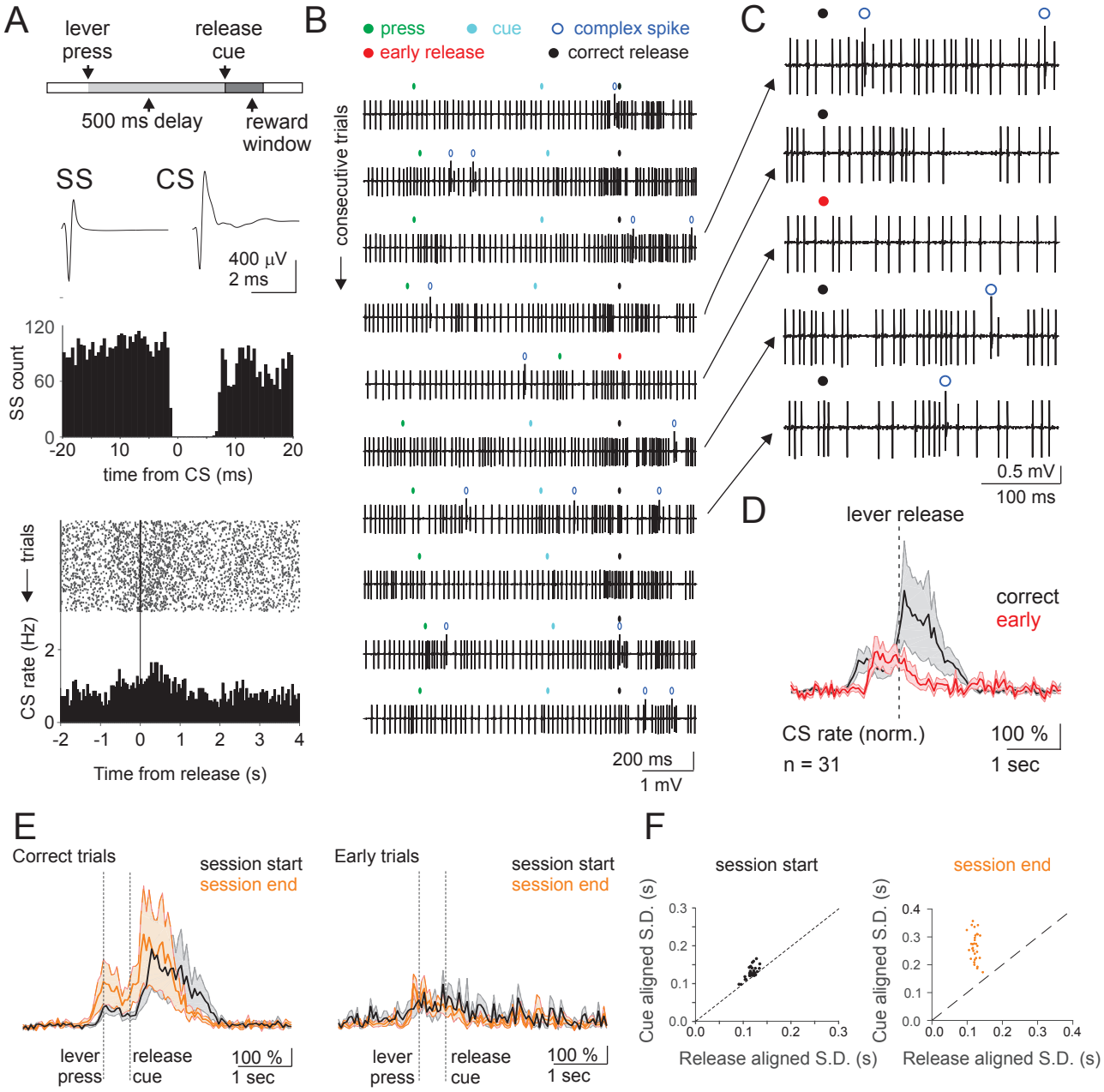

mean release aligned S.D. = 0.118 ± 0.002
mean cue aligned S.D. = 0.130 ± 0.003
p =3.7e-06

mean release aligned S.D = 0.123 ± 0.002
mean cue aligned S.D. = 0.265 ± 0.009
p = 1.7e-15

supplemental figure 6

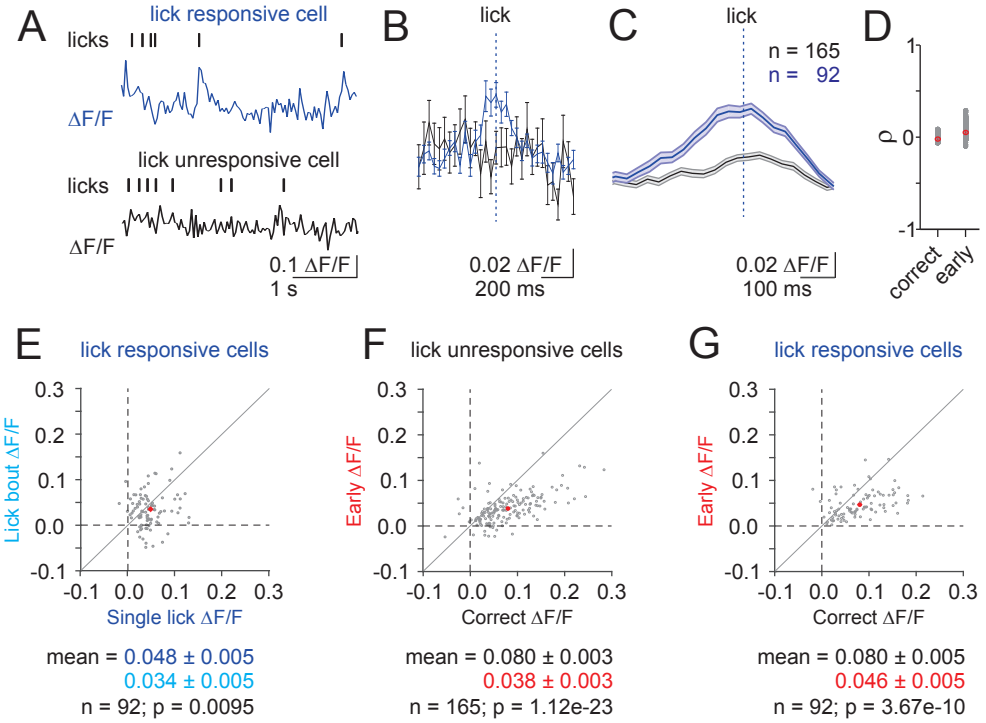

supplemental figure 7

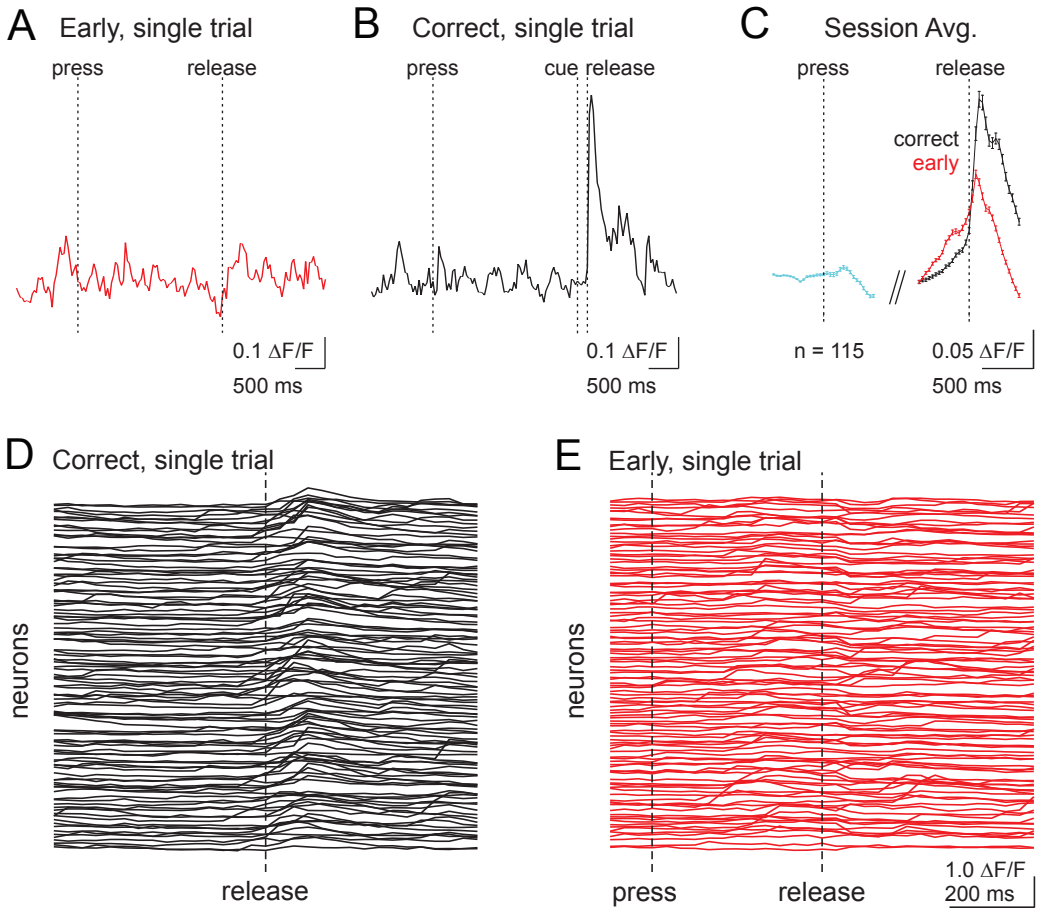

supplemental figure 8

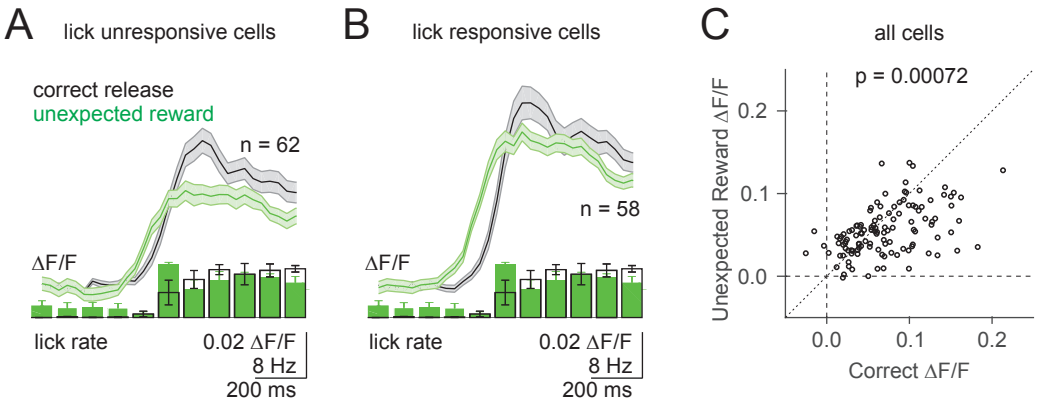

supplemental figure 9

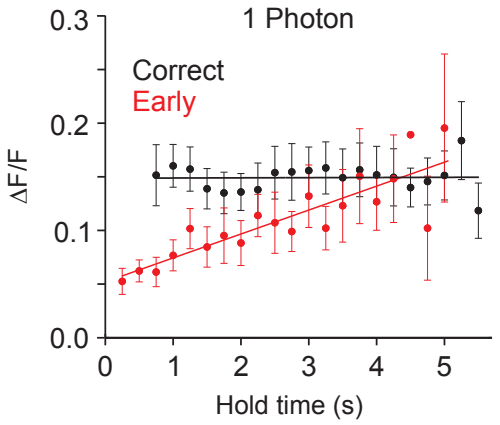

supplemental figure 10

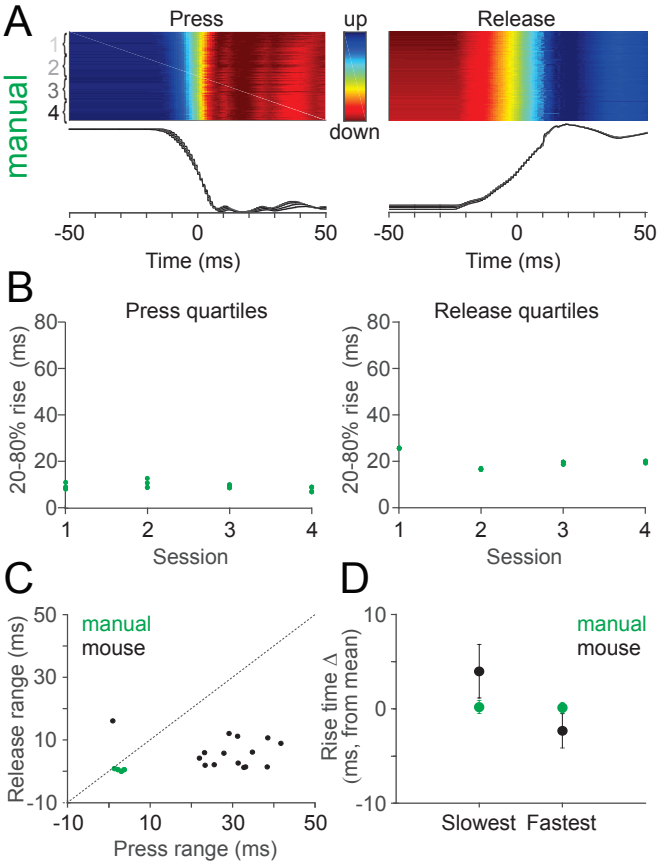

supplemental figure 11